Asian Journal of Research and Reviews in Physics

1(2): 1-35, 2018; Article no.AJR2P.41729

Comparison of Iron Plasma Atomic and Radiative Properties Computed with a Relativistic Collisional Radiative Average Atom Code versus Other Models

A. J. Benita[1,2*]

[1]Plasma Atomic Physics Group, Madrid Polytechnic University, 28006 Madrid, Spain.
[2]Department of Physics, Las Palmas Canary Islands University, 35017 Las Palmas de Gran Canaria, Spain.

Author's contribution

The sole author designed, analyzed and interpreted and prepared the manuscript.

Article Information

DOI: 10.9734/AJR2P/2018/v1i224599
Editor(s):
(1) Vitalii A. Okorokov, Professor, Department of Physics, National Research Nuclear University MEPhI, (Moscow Engineering Physics Institute) – NRNU MEPhI, Moscow, Russia.
Reviewers:
(1) Pain Jean-Christophe, France.
(2) Hulin Huang, Nanjing University of Aeronautics and Astronautics, P.R. China.
Complete Peer review History: http://www.sciencedomain.org/review-history/24863

Original Research Article

Received 17th March 2018
Accepted 25th May 2018
Published 29th May 2018

ABSTRACT

In this paper, it is presented a representative sample of steady state iron plasmas focusing the attention on two issues. First, the huge computation capability extension up to millions of plasmas with the implementation of a collisional radiative balance in the relativistic average atom model ATMED. Second, it will be addressed the good agreement of atomic and radiative properties not only with respect to very recent experimental measurements of laboratories and High Energy Density facilities, but also to the last theoretical developments in quantum mechanics of statistical methods, as new codes based on the self consistent Hartree-Fock-Slater model for the average atom which in turn solve the Schrödinger's or Dirac's equations of radial wave functions. The new codes have been validated with some state of the art models as OPAL, SCO-RCG, STA, CASSANDRA, LEDCOP, THERMOS, etc.
The results for plasma properties can be considered as relatively precise and optimal, being checked fundamentally the high sensitivity of calculations to changes in regime, local thermodynamic equilibrium (LTE) or non-LTE (NLTE), electronic and radiation temperatures, dilution

**Corresponding author: E-mail: anajosefa.benita@upm.es;*

factor, matter or electronic density and plasma length. The systematic theoretical investigation is carried out through comparison of calculations performed with a wide set of atomic collisional radiative codes with detailed configurations or codes of the average atom formalism. Some transmissions computed with ATMED CR using UTA (Unresolved Transition Array) formalism are also checked with respect to very recent experimental measurements of laboratories.

Keywords: Screened hydrogenic atomic model; collisional radiative average atom code; steady state iron plasmas; wide thermodynamic ranges.

1. INTRODUCTION

The collisional radiative model ATMED CR [1,2] constructed in the Average Atom formalism has been developed to calculate plasma population kinetics under coronal, local or non-local thermodynamic equilibrium regimes as an extension of the module named ATMED LTE [3-5] designed previously for local thermodynamic conditions. The atomic model is based on a New Relativistic Screened Hydrogenic Model (NRSHM) with a set of universal screening constants including *nlj*-splitting that has been obtained by fitting to a large database of 61,350 atomic high quality data entries, compiled from the National Institute of Standards and Technology (NIST) database of U.S. Department of Commerce and from the Flexible Atomic Code (FAC) [6,7].

The calculation of accurate relativistic atomic populations including *nlj*-splitting of electronic orbitals, improves the precision of atomic properties as mean charge, rates and the resolution of spectral properties as opacities and radiative power losses, with respect to collisional radiative average atom codes as XSN of W. Lokke and W. Grasberger of 1977 with *n*-splitting [8,9] or considering *nl*-splitting [10-13]. The CR balance is based on iterative loops for reaching auto convergence in populations and plasma mean charge [14]. The accuracy ATMED CR code can achieve can be consulted in Section 3 of Ref. [15] which explains in detail the phases of the investigation project, consisting of the comparison of plasma properties of this software with bibliographic data.

The implementation of the collisional radiative balance with the new atomic model, allows now to compute plasmas in NLTE regime or coronal regime, widening considerably for all chemical elements the validity range of thermodynamic conditions. Through a quantitative estimation, plasmas computed in LTE regime can imply only 15÷25% of the total number of non photoionized plasmas, that's to say, without an external radiation field. Performing also a gross calculation and adjusting formulas for very high temperatures, ATMED CR can model millions of plasmas of pure elements and of multiple combinations of volume percentages of elements in mixtures. Besides, for each value of electronic temperature T_e (eV) subdividing the logarithmic decades of input parameters within very narrow ranges, a lot of radiation temperatures and dilution factors can be considered.

Section 2 displays a summary of the chronology of average atom models evolution highlighting the progressive and gradual quantization of matter atomic structure through theoretical and programming development. In Section 3 there are modeled plasmas [*] with ATMED CR illustrating the huge extension got with the release of module ATMED CR in 2017. The departures from LTE regime are clearly observed when plasma properties are computed with module ATMED CR ($T_R = 0$ or $T_R \neq T_e$) in respect of calculating with ATMED CR ($T_e = T_R$). Section 4 contains main conclusions.

2. GENERAL DESCRIPTION OF THE AVERAGE ATOM MODEL ATMED

2.1 Average Atom Models Evolution & Generations

In this section can be found a gross summary of the average atom models evolution according to the progressive treatment of bound and free electrons in the ion-sphere model and according also to the quantum numbers with respect to splitting of the matter structure, of first generation with n-splitting (NOHEL, XSN [8]), of second generation with nl-splitting [10-13] and of third generation with nlj-splitting (THERMOS, ATMED LTE & CR, OPAQS, …) [16-32]. Highlighting some formulas, it can be noticed the long-term maintained evolution of atomic codes considering

[*] *Plasma properties of ATMED LTE/CR superimposed over some original figures (courtesy of References).*

the average atom as a statistical item of energy configuration levels (ground state of minimum energy, single excited, doubly excited, autoionizing level, etc.), inside each ionic charge state within a set of the most populated ones by abundance representing the whole plasma, see Fig. 1.

The fundamental notation of atomic codes is as follows:

AA :	Average Atom.
DCA :	Detailed Configuration Accounting.
DLA :	Detailed Level Accounting.
DTA :	Detailed Term Accounting.
$RDCA$:	Reduced Detailed Configuration Accounting.
SCA:	Super Configuration Accounting.
STA:	Super Transition Array.

In 1949, L. Thomas and E. Fermi established the first ion-sphere model in plasma physics without matter quantization or discrete energy levels [16], considering an ideal gas of electrons under the effect of an external autocoherent potential $v(r)$.

The electronic density in the non relativistic case is:

$$n(r) = 2\int \frac{d^3p}{h^3}\left\{1\Big/\left(e^{\beta\left(\frac{p^2}{2m}-v(r)-\mu\right)}+1\right)\right\} \quad (1)$$

The electrostatic potential is created by the nucleus charge along with the distribution of electron charges depending on their relative coordinates (r, r') of position in space:

$$v_{el}(r) = \frac{Ze^2}{r} - e^2\int d^3r'\left\{\frac{n(r')}{|r-r'|}\right\} \quad (2)$$

The autocoherent potential considers also the Kohn-Sham's correlation of exchange potential v_{xc}:

$$v(r) = v_{el}(r) - v_{xc}(n(r)) \quad (3)$$

In 1972, B. Rozsnyai proposed a new average atom model considering nl-shells for the bound electrons in the ionic cell with discrete energy eigenvalues defined by quantum numbers (n,l,m), retaining an ideal gas of free electrons without quantization [16]:

$$n(r) = 2\sum_{n_r,l,m}\int_{E^-_{n_r,l}}^{E^+_{n_r,l}} dE\left\{f^F(E)\frac{3\sqrt{E}}{2(E^+_{n_r,l}-E^-_{n_r,l})^{3/2}}\left|\psi_{E,l,m}(r)\right|^2\right\} + \frac{8\pi}{h^3}\int_{p_0(r)}^{\infty} dp\left\{p^2\Big/\left(e^{\beta\left(\frac{p^2}{2m}-v(r)-\mu\right)}+1\right)\right\} \quad (4)$$

The CR model XSN of authors W.A. Lokke and W.H. Grasberger was released in 1977 [8], developed in LLNL (Lawrence Livermore National Laboratory, California, USA) and considering n-splitting of energy orbitals of the average atom based on a screened hydrogenic atomic model.

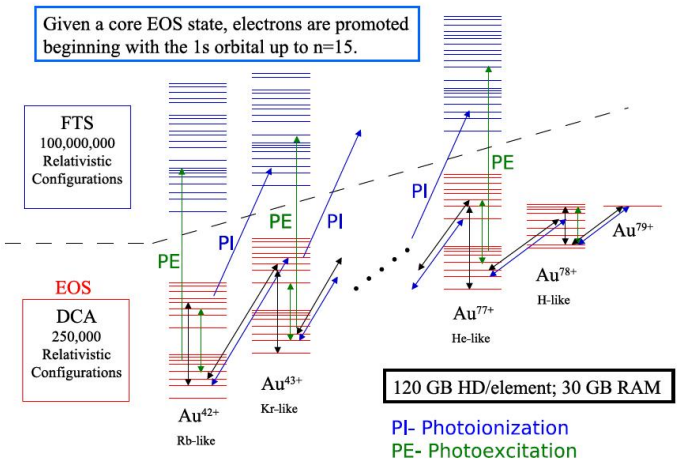

Fig. 1. Atomic and nuclear shell structure characterization. Ionic charge states of gold in plasmas with detailed codes [24]

In 1979, the INFERNO model by D.A. Liberman [20] considered a quantum treatment for both, bound and free electrons also through the quantum numbers (n,l,m) and considering the Fermi energy distribution functions $f^F(E_{n_r,l})$ and $f^F(E)$ respectively:

$$n(r) = 2\sum_{n_r,l,m} f^F(E_{n_r,l})\left|\psi_{n_r,l,m}(r)\right|^2 + 2\sum_{l,m}\int dE\left\{f^F(E)\left|\psi_{E,l,m}(r)\right|^2\right\} \quad (5)$$

Other quantum models of Atom in Jellium (Atome dans un Jellium de Charge Imposée, AJCI) formalism were developed during decades of 90's and 2000, as CASSANDRA [21,22], PURGATORIO [23], VAAQP [16] or the collisional radiative codes with nl-splitting of References [10-13].

In 2011, M.A. Mendoza launched ATMED LTE with a doctoral thesis [4,5] based on the New Relativistic Screened Hydrogenic Atomic Model (NRSHM) considering the next equation for a gas of free degenerated electrons:

$$f_{1/2}(\eta_e^0) = Z_{bar}^0\left[\frac{4}{\sqrt{\pi}}\frac{A}{\rho N_A}\left(\frac{m_e k_B T_e}{2\pi\hbar^2}\right)^{\frac{3}{2}}\right]^{-1} \quad (6)$$

Bound electrons are characterized through relativistic P. Dirac's energy eigenvalues ε_k for bound states, depending on screened charges Q_k for each relativistic level k of the average atom:

$$\varepsilon_k = m_e c^2\left[\left(1+\left[\frac{\alpha Q_k}{n-j-1/2+\sqrt{(j+1/2)^2-(\alpha Q_k)^2}}\right]^2\right)^{-1/2}-1\right] \quad (7)$$

Screened charges Q_k are calculated depending on screening constants $\sigma_{kk'}$, relativistic orbital populations P_k and energy levels degeneracy D_k considering ionization pressure as model for plasma effects:

$$Q_k = Z - \sum_{k=1}^{k\max}\sigma_{kk'}\left(1-\frac{\delta_{kk'}}{D_k}\right)P_{k'} \quad (8)$$

Wavefunctions of bound electrons can be also computed based on screened charges Q_k:

2.2 Module ATMED CR

In 2017, ATMED CR is released with a doctoral thesis, with the computation capability of millions of plasmas with very optimal and relatively precise results performing calculations with atomic processes rates inside an iterative collisional radiative balance [2,14]. Although being screened hydrogenic and performing calculations based on formulas instead on values of databases, the atomic NRSHM used inside the collisional radiative balance of ATMED CR has a very good agreement in respect of atomic and radiative properties with results of other codes, that solve numerically or analytically the non relativistic equation of E. Schrödinger and the relativistic equation of P. Dirac for medium and highly ionized atoms, see "APPENDIX III" of Reference [14]. The implementation of the collisional radiative balance has widened the validity range of thermodynamic conditions, as it can be observed in Fig. 3 for the examples of carbon and xenon. The non-LTE effects are noticeable for high densities with increasing temperatures depending also on increasing atomic numbers (Z).

3. MODELING OF STEADY STATE IRON PLASMAS

3.1 Atomic Properties

3.1.1 Mean Charge

In Fig. 4 and Table 1 there are displayed mean charge values of iron plasmas, checking the high agreement of ATMED CR results with respect to other atomic codes [9,17,27-29], being as well as a snapshot of the high sensitivity to slight changes in temperatures or densities. The departures from LTE regime are clearly observed with ATMED CR for low densities, high temperatures or T_R = 0 eV.

In Fig. 4.b there are displayed mean charge values of iron plasmas, checking the high agreement of ATMED CR (—) at N_{ion} = 1E+18 cm^{-3}, (—) at N_{ion} = 1E+20 cm^{-3}, (—) at N_{ion} = 1E+22 cm^{-3} results with respect to other atomic codes D (—), R10 (—), R30 (—) and XSN (—) of Ref. [9], also as a snapshot of the high sensitivity to changes in temperatures $T_e \neq T_R$ eV (Tr = T_R) or densities.

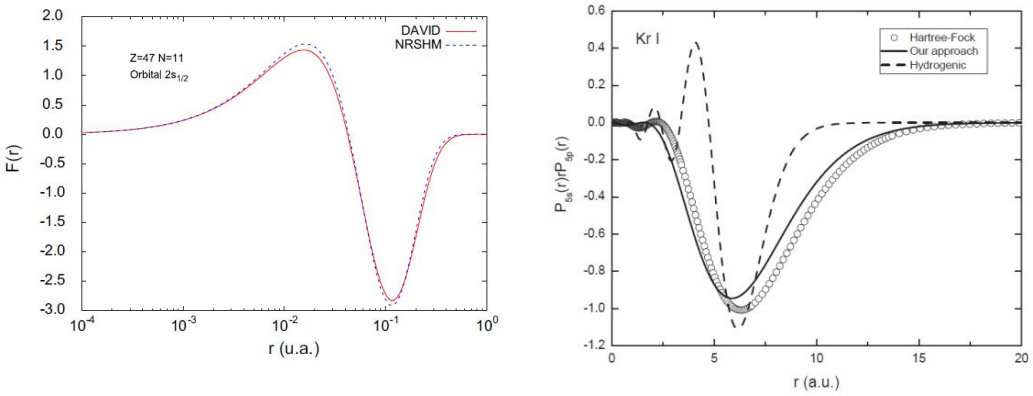

Fig. 2. Wavefunctions of ATMED according to formulas in references [6] and [19] for plasmas of Na-like Ag and Kr I (Our approach)

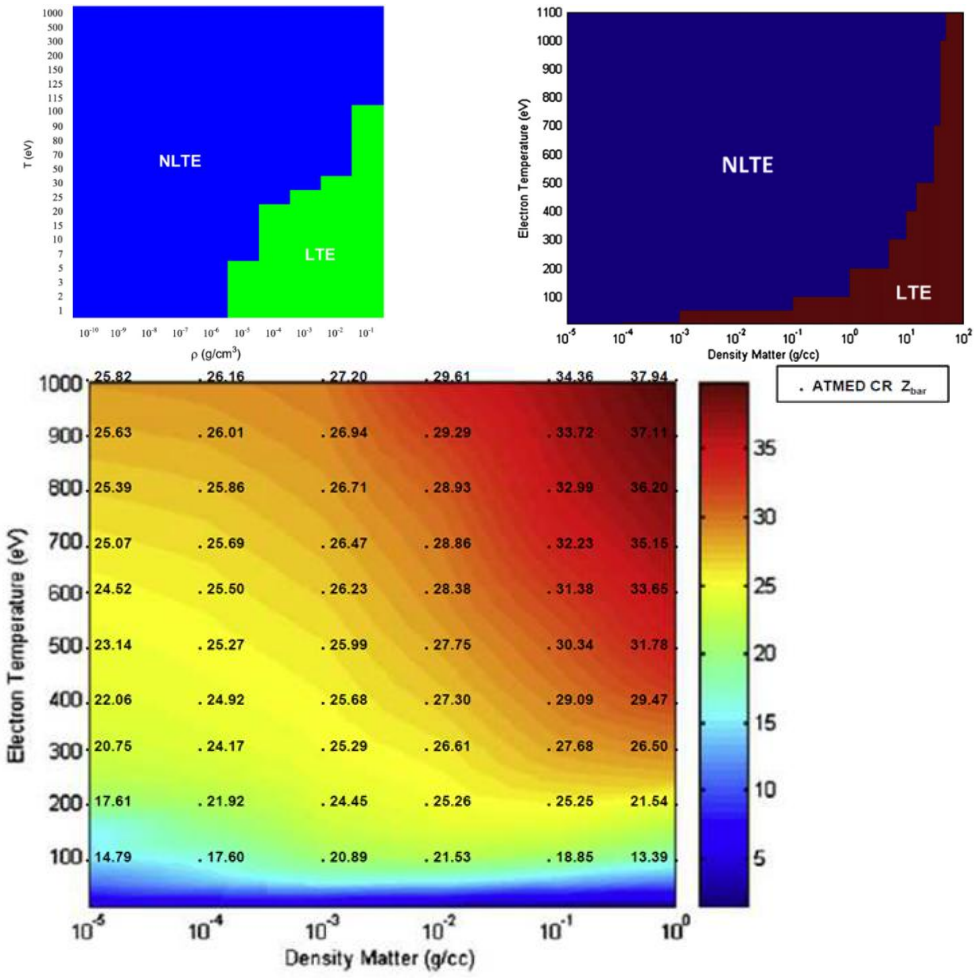

Fig. 3. Regime maps of code ABAKO for C [25] and Xe [26] plasmas. Xenon mean charge Z_{bar} colour map of ABAKO and ATMED CR [2]

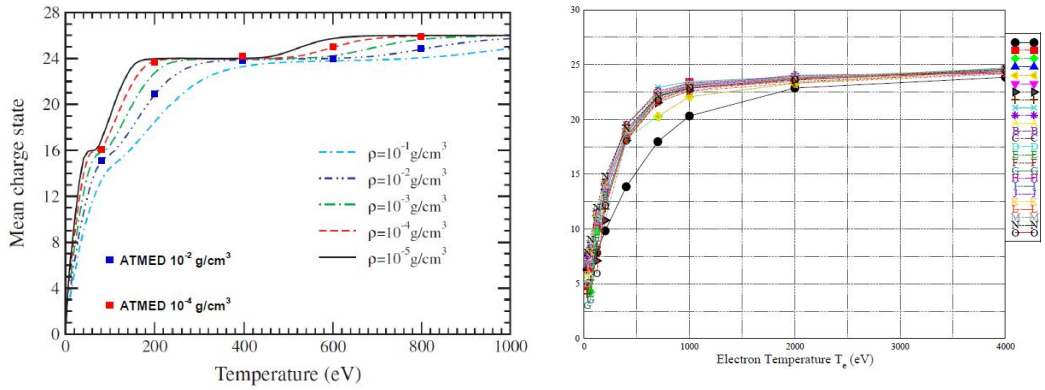

Fig. 4.a. Mean charge state Z_{bar} of iron plasmas versus electronic temperature T_e and several densities with codes ATMED LTE, 10^{-2} g/cm^3 (■) or 10^{-4} (■), and of Ref. [27] (left). Z_{bar} versus T_e and N_e=1E+24 cm^{-3} with ATMED CR (■) and other codes of Workshop NLTE-9 [17]

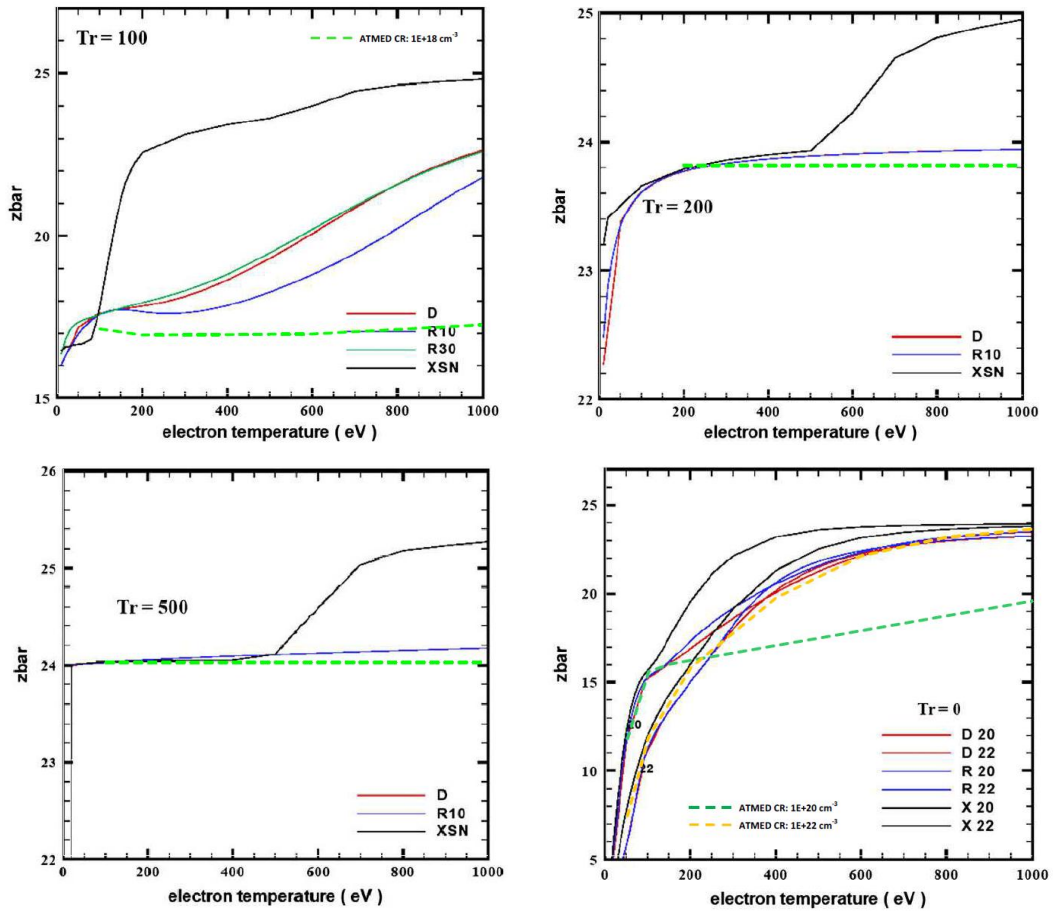

Fig. 4.b. Mean charge state Z_{bar} of iron plasmas versus electronic temperature T_e and several atom number densities (ionic densities): N_{ion} = 1E+18 cm^{-3} with Tr=100, 200, 500 eV; N_{ion} = 1E+20, 1E+22 cm^{-3}, Tr=0 with codes ATMED CR, D (–), R10 (–), R30 (–) and XSN (–) [9]

Table 1.a. Evolution of variable mean charge Z_{bar} with ATMED CR for comparison with ATMED LTE and codes of Ref. [9,17,27-29]

ATMED LTE T_e (eV)	**80**	**200**	**400**	**600**	**800**	**1000**
ρ (g/cm^3) = 10^{-2}	15.16	20.99	23.95	24.03	24.82	25.75
ρ (g/cm^3) = 10^{-4}	16.20	23.78	24.00	24.97	25.96	26.00
ATMED CR T_e=T_R	**80**	**100**	**200**	**400**	**800**	**1000**
ρ (g/cm^3) = 10^{-2}	15.16	15.74	20.77	23.94	24.79	25.74
ρ (g/cm^3) = 10^{-4}	16.21	17.49	23.77	24.00	25.96	26.00
ATMED CR T_R=0	**80**	**100**	**200**	**400**	**800**	**1000**
ρ (g/cm^3) = 10^{-2}	14.58	15.46	16.02	16.60	18.83	19.54
ρ (g/cm^3) = 10^{-4}	12.88	13.45	15.43	15.84	16.08	16.19
CODE ρ (g/cm^3)= 1	**CASSANDRA**	**LEDCOP**	**OPAQS**	**ATMED LTE**	**ATMED CR T_e=T_R**	**ATMED CR T_R=0**
T_e (eV) = 500	22.32	22.68	22.41	22.29	22.72	21.05
T_e (eV) = 1000	23.91	23.94	23.97	23.87	24.08	23.55
ρ (g/cm^3)= 0.0127	**CASSANDRA**	**LEDCOP**	**OPAQS**	**ATMED LTE**	**ATMED CR T_e=T_R**	**ATMED CR T_R=0**
T_e (eV) = 59	12.49	12.83	12.89	12.94	12.93	12.59
ρ (g/cm^3)= 7.86	**CASSANDRA**	**LEDCOP**	**OPAQS**	**ATMED LTE**	**ATMED CR T_e=T_R**	**ATMED CR T_R=0**
T_e (eV) = 200	14.68	14.42	14.42	14.17	13.53	13.52

Table 1.b. Evolution of variable mean charge Z_{bar} with ATMED CR for comparison with codes of Ref. [9]

N_{ion} (cm^{-3}) = 10^{18}	**T_e = 100**	**T_e = 200**	**T_e = 400**	**T_e = 600**	**T_e = 1000**
Tr (eV) = 100	1.748E+01	1.681E+01	1.674E+01	1.684E+01	1.712E+01
Tr (eV) = 200	2.165E+01	2.371E+01	2.373E+01	2.375E+01	2.380E+01
Tr (eV) = 500	2.400E+01	2.400E+01	2.400E+01	2.400E+01	2.402E+01

Table 1.c. Evolution of variable mean charge Z_{bar} with ATMED CR for comparison with codes of Ref. [9]

N_{ion} (cm^{-3}) = 10^{20}	**T_e = 50**	**T_e = 100**	**T_e = 150**	**T_e = 400**	**T_e = 600**	**T_e = 800**	**T_e = 1000**
Tr (eV) = 0	1.163E+01	1.546E+01	1.589E+01	1.633E+01	1.677E+01	1.727E+01	1.946E+01
N_{ion} (cm^{-3}) = 10^{22}	**T_e = 50**	**T_e = 100**	**T_e = 200**	**T_e = 400**	**T_e = 600**	**T_e = 800**	**T_e = 1000**
Tr (eV) = 0	7.244E+00	1.175E+01	1.570E+01	1.965E+01	2.202E+01	2.309E+01	2.355E+01

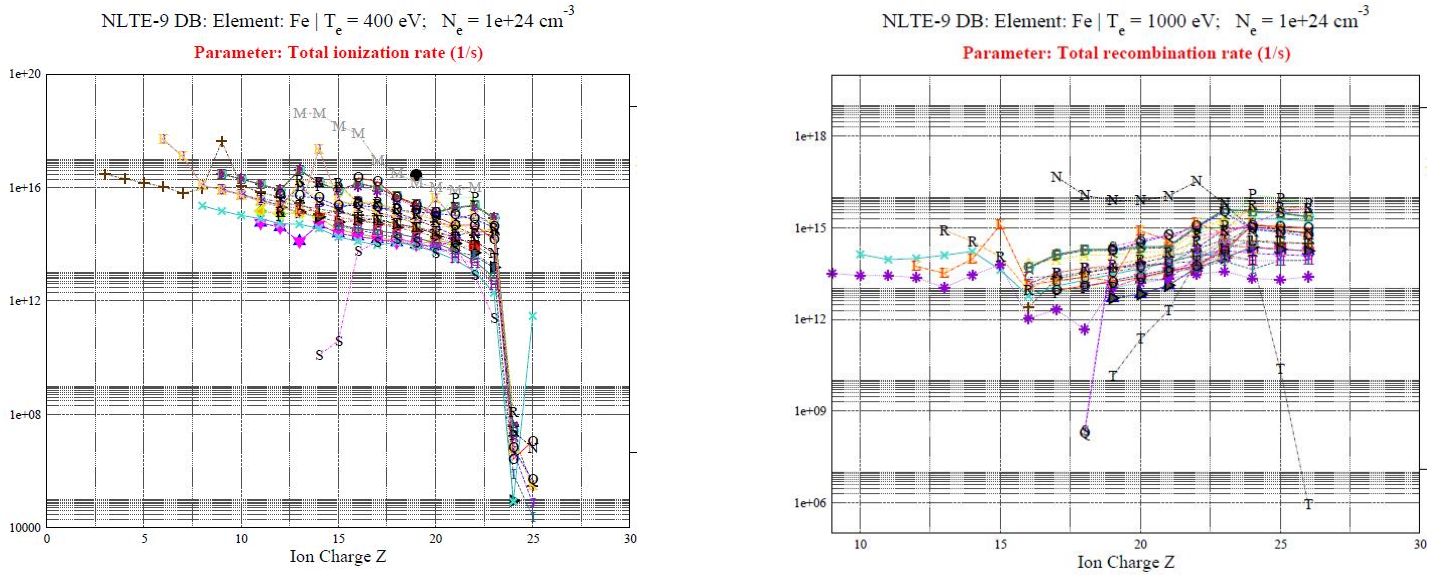

Fig. 5. Total ionization and recombination rates of ATMED CR (●) and codes of NLTE-10 Workshop, N_e = 1.0E+24 cm^{-3}, T_e = 400/1000 eV

Table 2.a. Total ionization rates with ATMED CR for comparison with codes of NLTE-10 Workshop at N_e = 1.0E+24 cm^{-3}, T_e = 400/1000 eV

Ion 400 eV	ATMED CR	ATOMIC_RCAL	AVERROES	CRAC	CRETIN_M	JATOM	SCRAM
18	0.000e+00	1.349e+14	3.951e+14	1.184e+14	4.782e+15	3.113e+16	1.822e+15
19	2.762e+16	1.044e+14	2.830e+14	8.717e+13	2.602e+15	1.553e+16	1.277e+15
20	0.000e+00	1.286e+14	1.870e+14	5.441e+13	1.350e+15	9.944e+15	8.948e+14
Ion 1000 eV	**ATMED CR**	**ATOMIC_RCAL**	**AVERROES**	**CRAC**	**CRETIN_M**	**JATOM**	**SCRAM**
22	0.000e+00	6.022e+13	4.829e+14	9.169e+13	9.890e+15	2.647e+17	7.896e+15
23	1.391e+16	2.248e+14	2.042e+14	2.481e+13	3.482e+15	8.675e+15	1.090e+15
24	0.000e+00	2.810e+11	1.748e+11	1.741e+10	2.501e+12	1.083e+12	9.478e+11

Table 2.b. Total recombination rates of ATMED CR for comparison with codes of NLTE-10 Workshop, N_e = 1.0E+24 cm^{-3}, T_e =400/1000 eV

Ion 400 eV	ATMED CR	ATOMIC_RCAL	AVERROES	CRAC	CRETIN_M	JATOM	SCRAM
18	0.000e+00	1.118e+14	3.798e+14	1.289e+13	3.318e+15	2.316e+16	1.492e+15
19	1.098e+15	1.521e+14	5.173e+14	1.192e+14	2.934e+15	1.988e+16	1.383e+15
20	0.000e+00	2.127e+14	6.540e+14	1.514e+14	2.795e+15	2.331e+16	1.531e+15
Ion 1000 eV	**ATMED CR**	**ATOMIC_RCAL**	**AVERROES**	**CRAC**	**CRETIN_M**	**JATOM**	**SCRAM**
22	0.000e+00	4.439e+13	1.959e+14	2.990e+13	1.042e+15	3.217e+16	1.065e+15
23	1.136e+14	2.501e+14	4.170e+14	3.720e+13	3.887e+15	6.043e+15	3.222e+15
24	0.000e+00	2.212e+14	3.641e+14	2.188e+13	3.442e+15	8.622e+14	9.175e+14

Table 3.a. Mean opacities with ATMED UTA modules LTE/CR for comparison with codes of Fig. 10

ATMED: T_e & ρ	LTE - K_R	CR - K_R $T_e = T_R$	CR - K_R $T_R = 0$	LTE - K_P	CR - K_P $T_e = T_R$	CR - K_P $T_R = 0$
100 eV & 0.1 g/cm^3	9.2666E+02	1.152E+03	1.216E+03	2.6908E+03	3.918E+03	4.036E+03
150 eV & 0.1 g/cm^3	3.3977E+02	3.913E+02	5.372E+02	1.9676E+03	2.748E+03	3.118E+03
200 eV & 0.1 g/cm^3	2.9358E+02	3.274E+02	5.487E+02	1.7816E+03	2.576E+03	3.621E+03
ATMED: T_e & ρ	**LTE - K_R**	**CR - K_R $T_e = T_R$**	**CR - K_R $T_R = 0$**	**LTE - K_P**	**CR - K_P $T_e = T_R$**	**CR - K_P $T_R = 0$**
100 eV & 0.01 g/cm^3	1.8650E+02	2.331E+02	3.833E+02	1.3152E+03	1.827E+03	2.253E+03
150 eV & 0.01 g/cm^3	8.4429E+01	2.600E+02	2.500E+02	1.3037E+03	2.478E+03	2.874E+03
200 eV & 0.01 g/cm^3	5.8886E+01	5.922E+01	3.282E+02	9.5787E+02	1.390E+03	3.804E+03
ATMED: T_e & ρ	**LTE - K_R**	**CR - K_R $T_e = T_R$**	**CR - K_R $T_R = 0$**	**LTE - K_P**	**CR - K_P $T_e = T_R$**	**CR - K_P $T_R = 0$**
100 eV & 0.001 g/cm^3	3.1294E+01	1.096E+02	4.460E+02	9.7028E+02	1.410E+03	2.468E+03
150 eV & 0.001 g/cm^3	1.7069E+01	1.851E+01	2.250E+02	7.5006E+02	1.041E+03	2.985E+03
200 eV & 0.001 g/cm^3	6.1002E+00	6.512E+00	3.280E+02	3.5010E+02	5.014E+02	4.000E+03

3.1.2 Atomic processes rates

The radiative and collisional rates for atomic processes between energy levels of the average atom are a good equilibrated set of analytical approximations of quantum mechanical ones. The *nlj*-splitting of orbitals improves the computation of electron binding energies, radial dipole matrix elements, multiplications of degeneracy and oscillator strengths *gf*-values and transition probabilities. In iron plasmas of NLTE-10 Workshop [17,18], the total rates of ionization and recombination have been included in the average ion according to plasma mean charge computed with ATMED CR (●), keeping high concordance in the order of magnitude with the rate figures for ions of different charge states calculated with detailed collisional radiative codes, see Fig. 5 and Table 2.

3.2 Radiative Properties

3.2.1 Spectrally resolved emission

In Fig. 6 there are displayed spectra of frequency resolved emission of iron plasmas of NLTE-10 Workshop [17,18]. For these plasma cases, ATMED CR obtains a spectrum UTA or MUTA (Mixed Unresolved Transition Array) below that one of detailed codes but above the spectrum of code CRETIN_M (—). CRETIN is a 1D, 2D and 3D non-local thermodynamic equilibrium (NLTE) atomic kinetics/radiation transport code of LLNL which follows the time evolution of atomic populations and photon distributions as radiation interacts with a plasma. It can provide detailed spectra for comparing with experimental diagnostics.

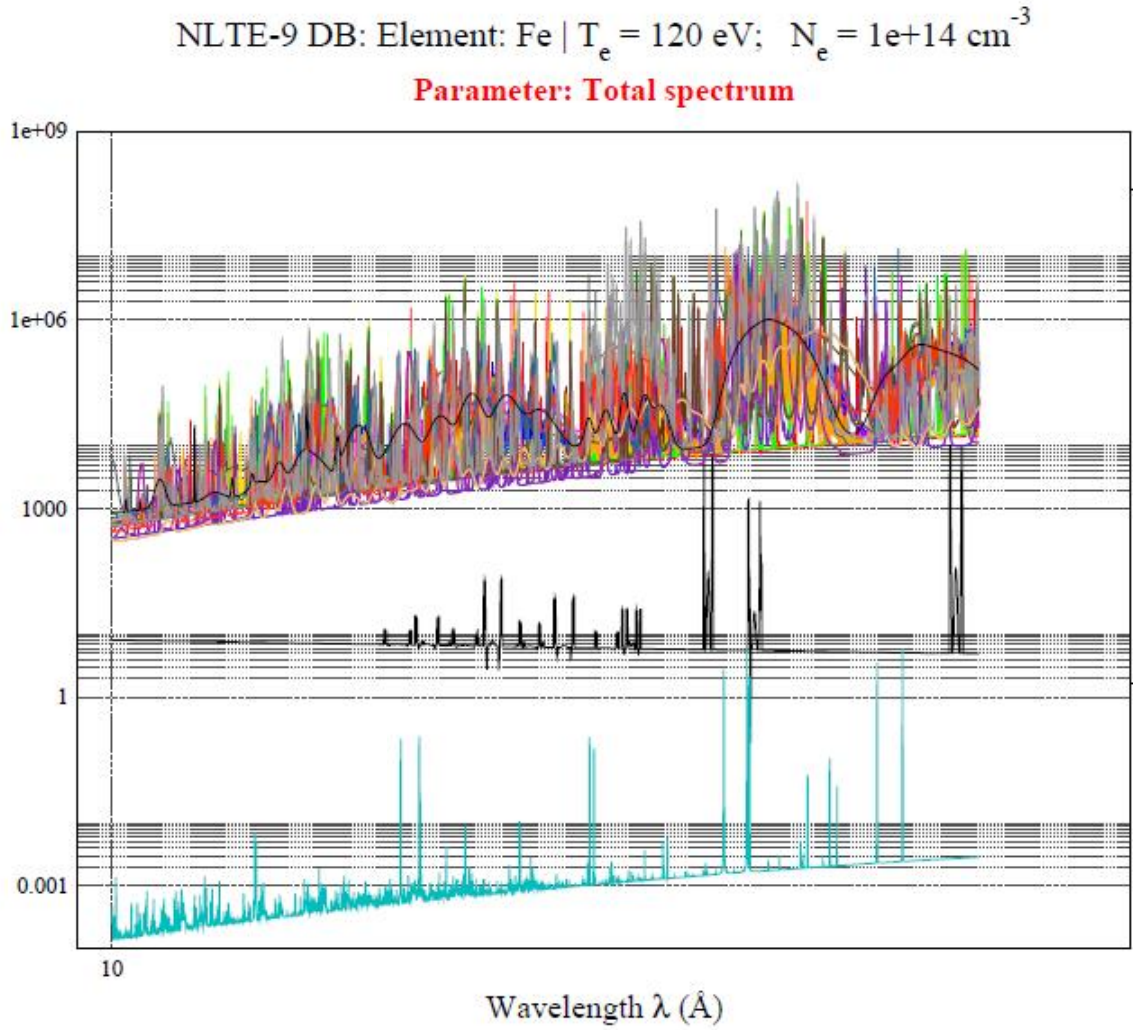

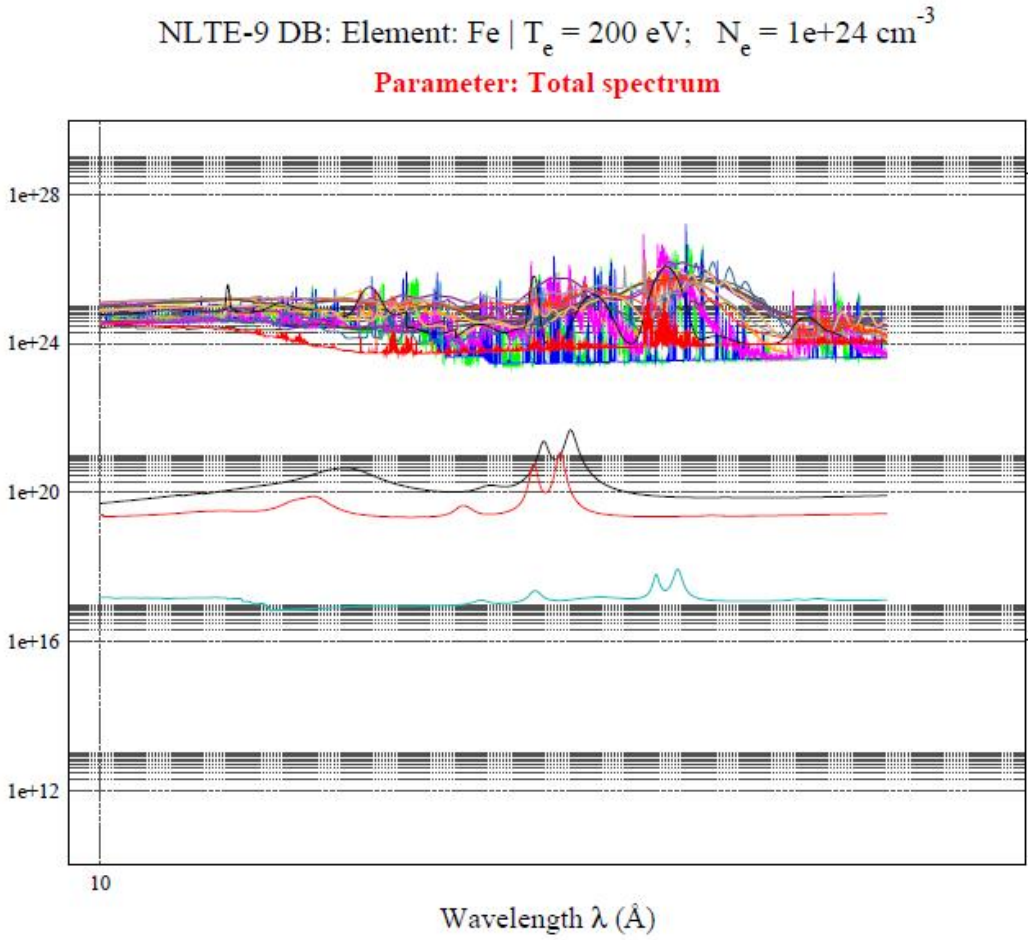

Fig. 6. Total emission spectra of ATMED CR MUTA (—) (above), or UTA (—), CRETIN_M (—) and other codes of NLTE-10 Workshop

3.2.2 Spectrally resolved & mean opacities of pure iron

In Figs. 7-12 there are displayed spectra of frequency resolved opacity (cm^2/g) of iron plasmas, checking the high spectral quality of ATMED CR with respect to other atomic codes [27-33], as well as the high sensitivity to slight changes in temperatures, densities or dilution factors.

ATMED CR code is very fast, for iron plasma case at T_e = 30 eV, T_R = 100 eV and ρ = 0.091 g/cm^3, the computation times are 581 s (DCA), 36 s (RDCA), 7.5 s (ATMED) and 1 s (XSN). For conditions T_e = 3000 eV the computation time with ATMED is 83 seconds. In Fig. 8.a the opacity profiles of ATMED CR UTA (—) are displayed at density 1 g/cm^3.

In Fig. 8.b the opacity profiles of ATMED CR of UTA, MUTA (—) formalisms are displayed, observing that the greater the electronic temperature T_e (1250 > 500) the greater the departure between calculations with radiation temperature $T_R = T_e$ (—) or T_R = 0 eV (—) and density 1 g/cm^3.

In Fig. 8.c opacity profiles of ATMED CR UTA are displayed, noticing the high sensitivity to changes in electronic temperature or dilution factor for specific plasmas at T_R = 800 or 250 eV.

In Fig. 9 the opacity profiles of ATMED LTE, ATMED CR (T_e=T_R) or (T_R=0) at T_e=80 eV and matter densities ρ = 0.01, 0.0001 g/cm^3 are shown and are also superimposed over ones in Ref. [27]. At low density 0.0001 g/cm^3 spectrum rises in NLTE regime (T_R=0) much more than

with 0.01 g/cm^3 in respect of the spectra with ATMED LTE or CR (T_e=T_R). It is observed also how the UTA spectra are a relatively good average of MUTA spectra.

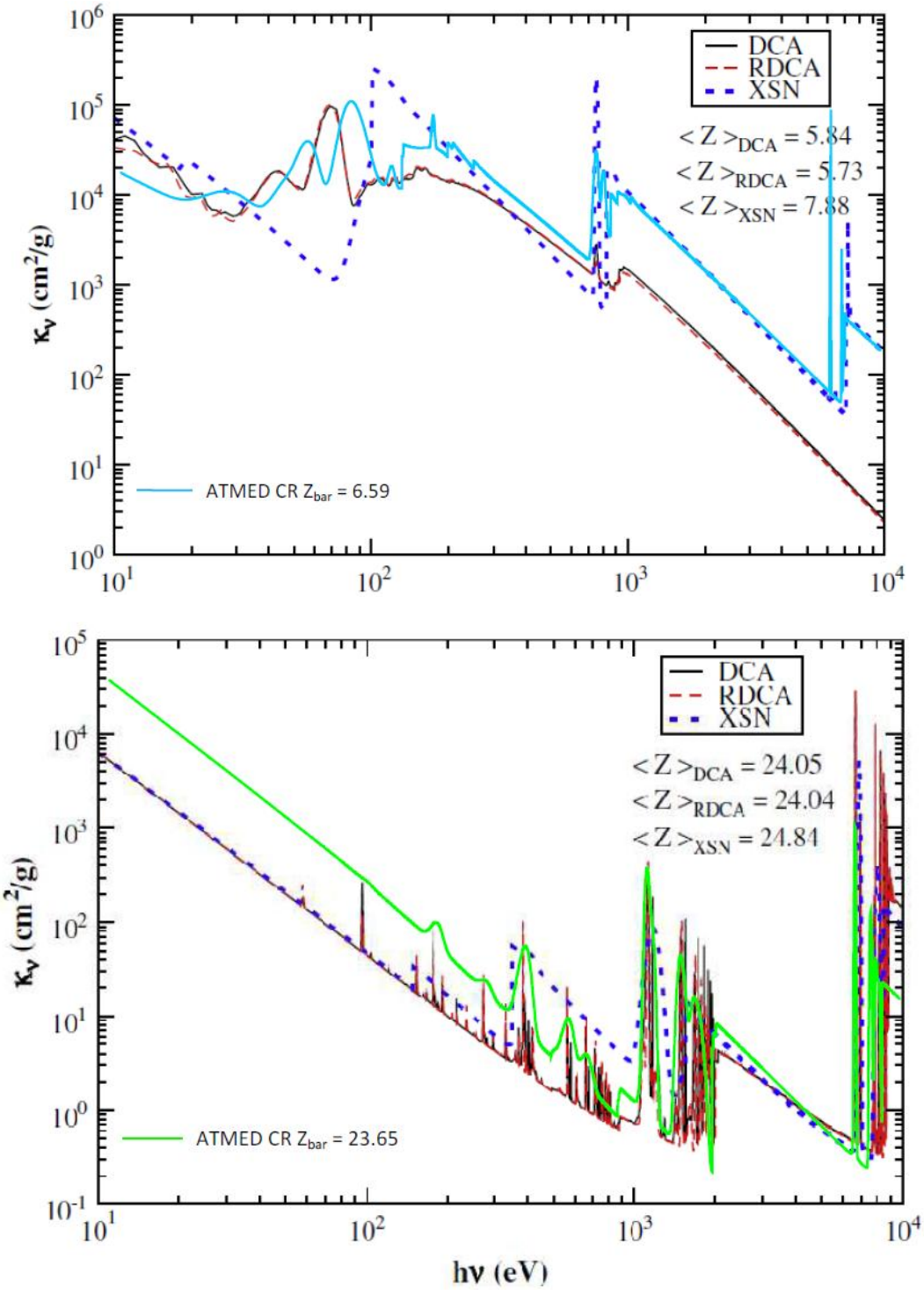

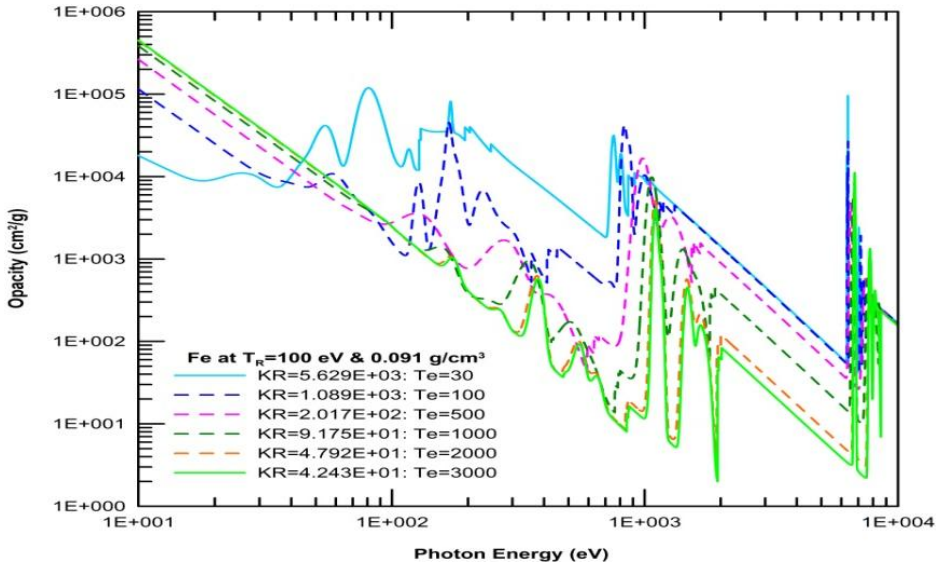

Fig. 7. Spectrally total resolved and mean K_R opacities of Fe plasmas at electronic temperature T_e = 30 (upper graph) or 3000 eV (intermediate graph), matter density ρ = 0.091 g/cm^3 and radiation temperature T_R = 100 eV with codes DCA, RDCA, XSNQ-U [30] and ATMED CR [1,2] with UTA formalism in NLTE. Spectrally total resolved opacity of iron plasmas at electronic temperature in the range T_e = 30÷3000, ρ = 0.091 g/cm^3 and radiation temperature T_R = 100 eV with code ATMED CR with UTA formalism in NLTE regime (below graph)

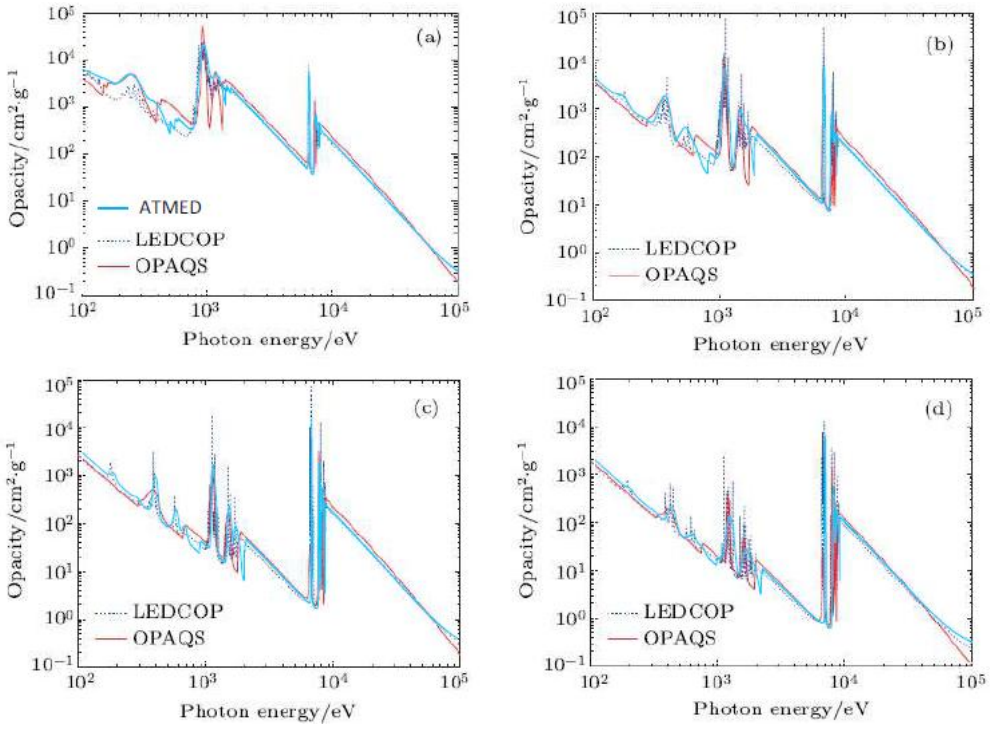

Fig. 8.a. Spectrally total resolved opacity of iron plasmas at electronic temperatures T_e = 250, 500, 800, 1250 eV and matter density ρ = 1 g/cm^3 with codes LEDCOP and OPAQS [28,29] and ATMED CR (—) with UTA formalism and radiation temperature T_R = T_e in LTE regime

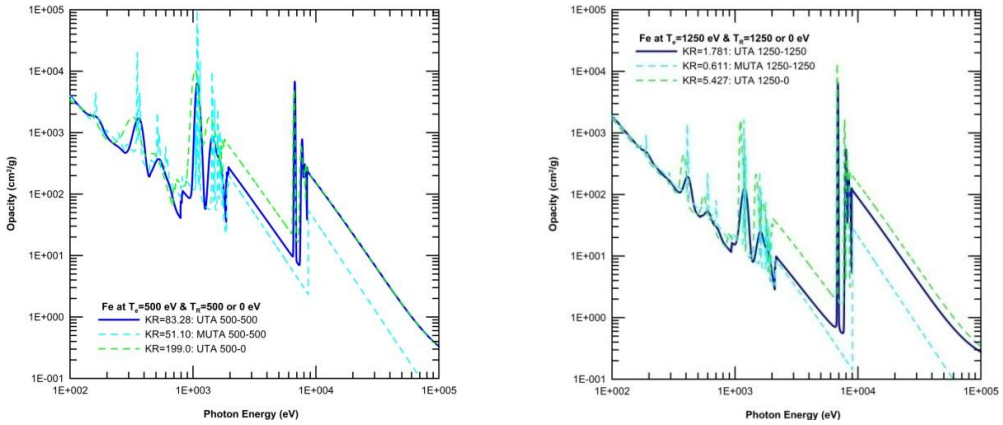

Fig. 8.b. Spectrally total resolved opacity and Rosseland mean opacity of iron plasmas at electronic temperatures T_e = 500 and 1250 eV and matter density ρ = 1 g/cm^3 with ATMED CR of UTA/MUTA formalisms and radiation temperature $T_R = T_e$ or 0 eV in NLTE/LTE regimes

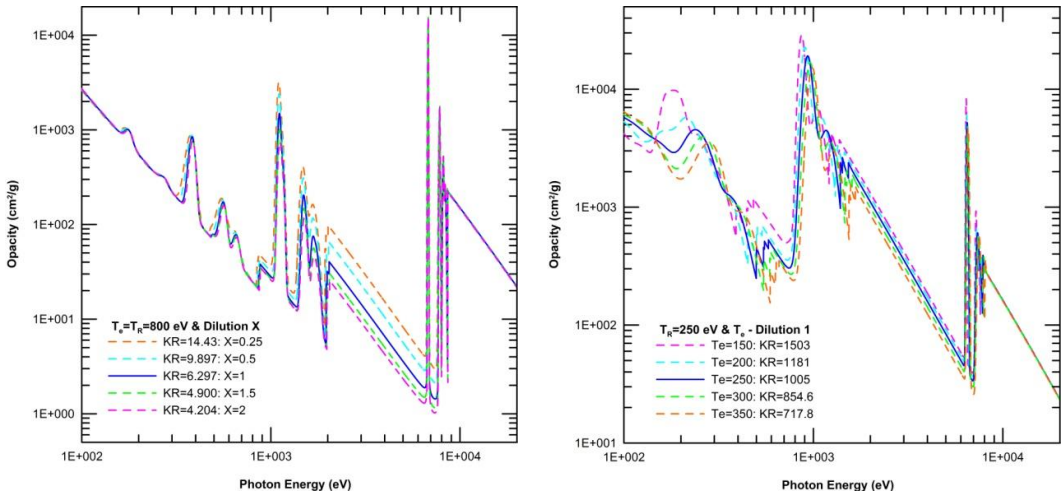

Fig. 8.c. Spectrally total resolved opacity and Rosseland mean of Fe plasmas and 1 g/cm^3 with code ATMED CR at radiation temperature T_R = 800, electronic temperature T_e = 800 eV and dilution factor X in the range 0.25÷2 (left) or T_R = 250, T_e in the range 150÷350 eV (right)

In Fig. 10 the opacity profiles of ATMED LTE at electronic temperature T_e = 100/150/200 eV and matter density ρ = 0.1 g/cm^3 (—), ρ = 0.01 g/cm^3 (—) and ρ = 0.001 g/cm^3 (—) are superimposed over spectra of Ref. [31]. The non-LTE effects are more significant the lower the density, the higher the temperature and can be observed when comparing calculations between ATMED LTE or ATMED CR ($T_e = T_R$) with respect to that of ATMED CR (T_R = 0).

In Fig. 10.c the opacity profiles of ATMED LTE, ATMED CR ($T_e = T_R$) and ATMED CR (T_R = 0) at electronic temperature T_e = 100/200 eV and matter density ρ = 0.1 (—), 0.01 (—) and 0.001 g/cm^3 (—) are displayed. The non-LTE effects can be observed vertically for decreasing densities at the same electronic temperature T_e, and also horizontally for increasing temperature at the same density.

In Figs. 11.a-b-c there are displayed spectra of frequency resolved opacity (cm^2/g) of iron plasmas for conditions of convection-radiation zone boundary, checking the high spectral quality of ATMED CR for very recent experimental measurements [34].

In Fig.11.c there are displayed frequency resolved opacities (cm^2/g) of iron plasma with ATMED CR UTA or MUTA, being mean charge

Z_{bar}=16.3 and opacities respectively K_R=935.3 / 553.5 cm^2/g.

In Fig. 11.d there are displayed frequency resolved opacities (cm^2/g) of iron plasma with ATMED CR UTA or MUTA belonging to cases of conditions in Reference [10], illustrating the sensitivity to radiation temperature T_R changes at electronic temperature T_e = 150 eV and density N_e = 2E+19 cm^{-3}.

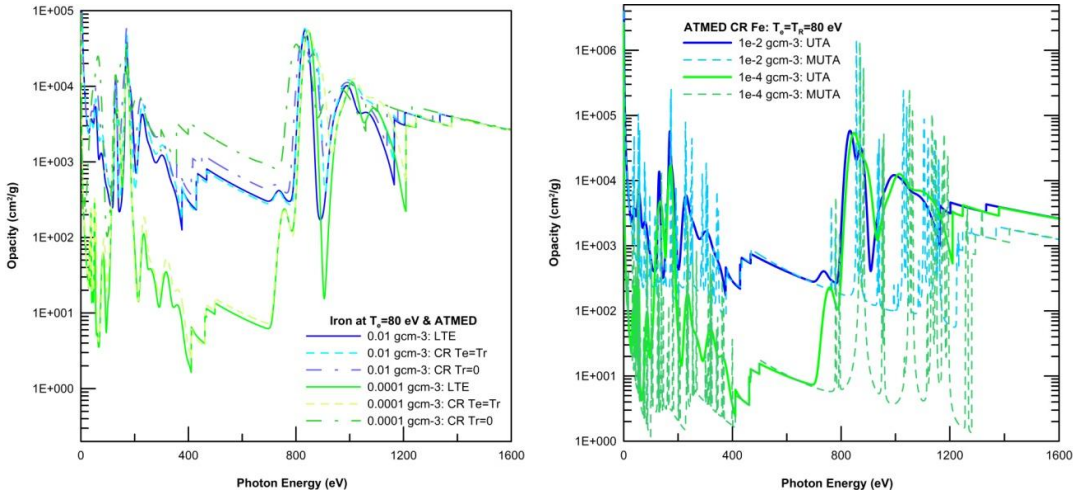

Fig. 9.a. Spectrally frequency resolved opacity of iron plasmas at electronic temperature T_e = 80 eV with ATMED LTE, ATMED CR (T_e = T_R) or ATMED CR (T_R =0) and matter densities 0.01, 0.0001 g/cm^3, and also with UTA/MUTA formalisms

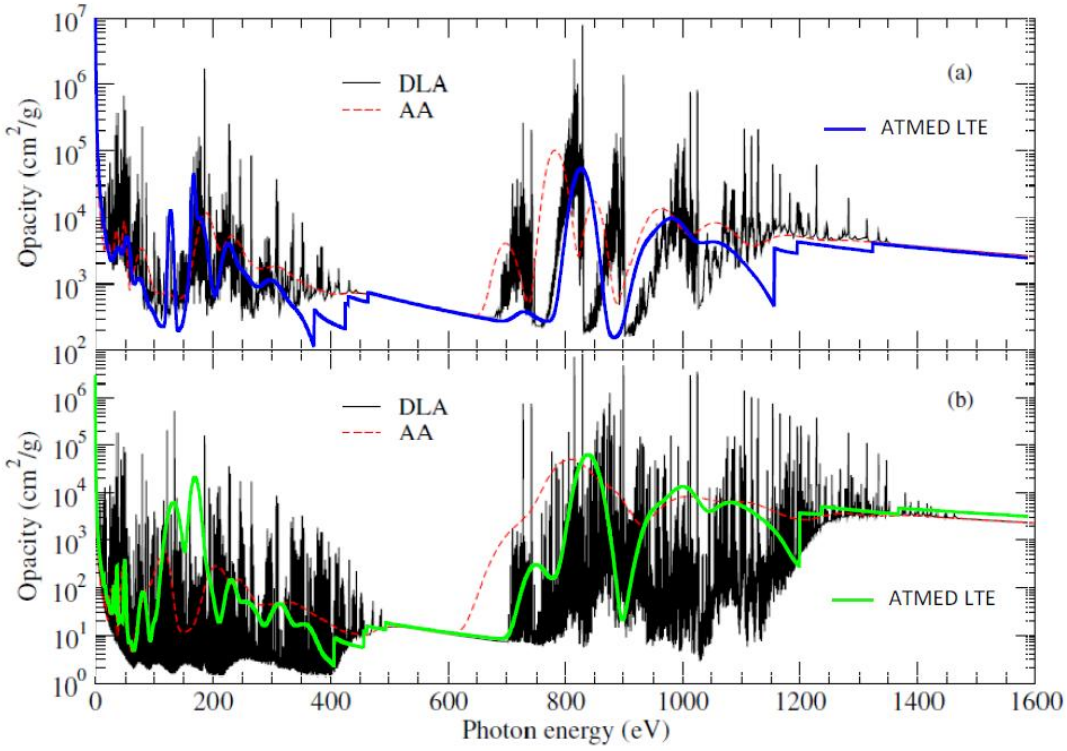

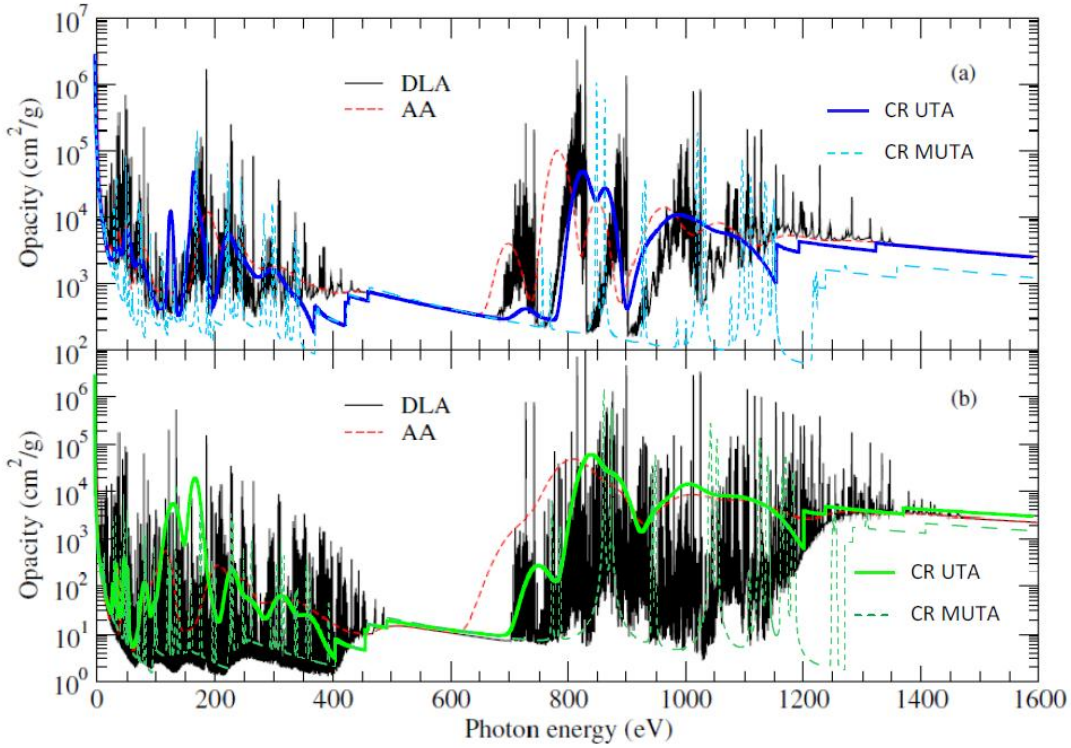

Fig. 9.b. Spectrally resolved opacity of iron plasmas at electronic temperature T_e = 80 eV, matter density with ATMED LTE/CR ($T_e = T_R$), (a) ρ = 0.01 g/cm^3 (—) and (b) ρ = 0.0001 g/cm^3 (—) in UTA/MUTA formalisms and codes detailed DLA (—) [27], average atom AA (—) [27]

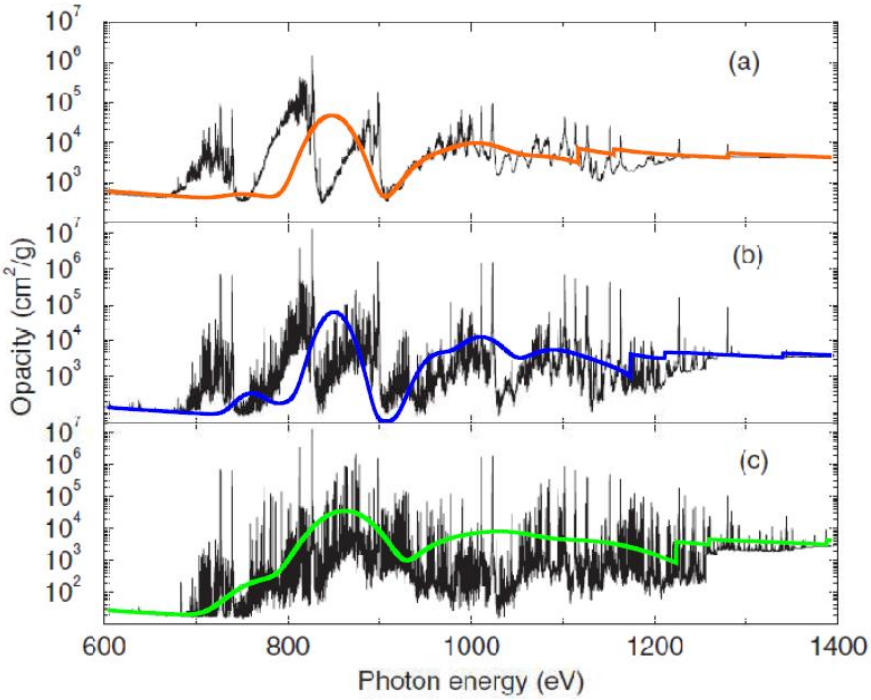

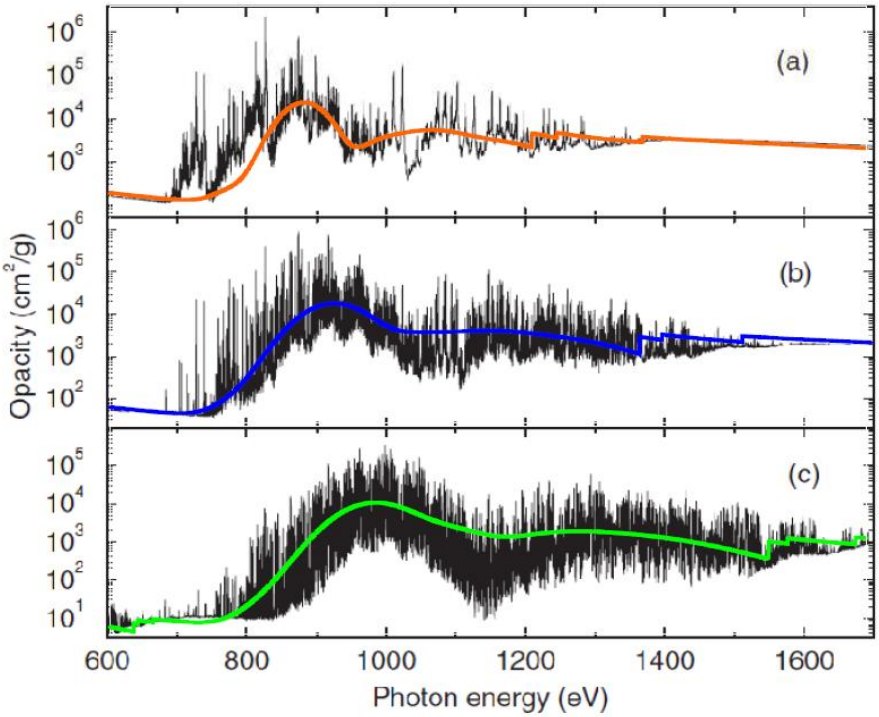

Fig. 10.a. Iron plasmas spectral opacity at electronic temperature T_e = 100/150 eV with ATMED LTE [3-5] and density (a) ρ = 0.1 g/cm^3 (—), (b) ρ = 0.01 g/cm^3 (—) and (c) ρ = 0.001 g/cm^3 (—) and also with code of Detailed Level Accounting formalism DLA (—) of Ref. [31]

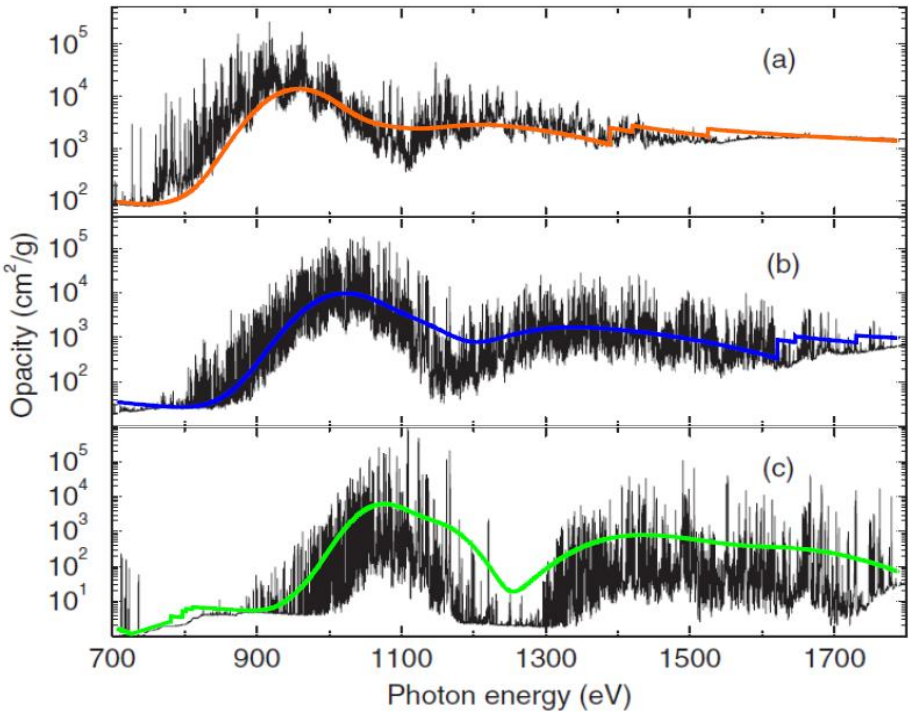

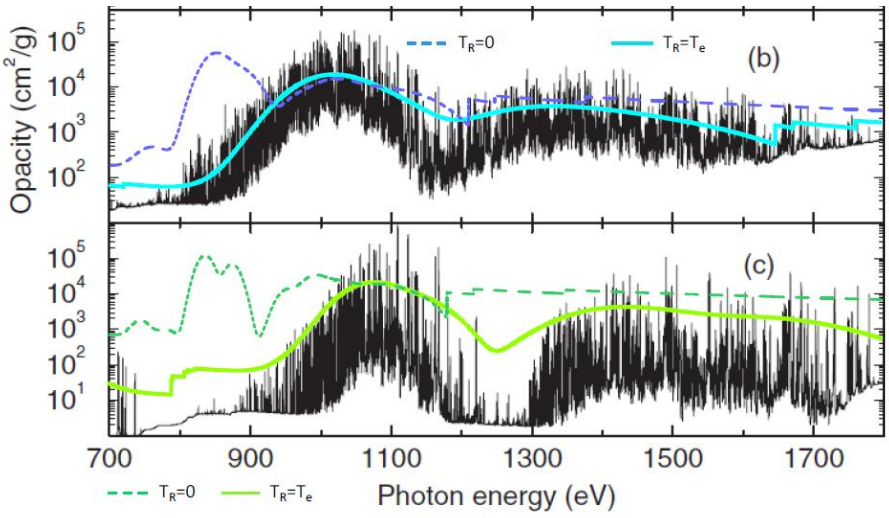

Fig. 10.b. Iron plasmas spectral opacity at electronic temperature T_e = 200 eV with ATMED LTE [3-5] and density (a) ρ = 0.1 g/cm^3 (—), (b) ρ = 0.01 g/cm^3 (—) and (c) ρ = 0.001 g/cm^3 (—), DLA (—) [31] and with ATMED CR UTA with same scale (b & c) and T_R=T_e or T_R=0 eV

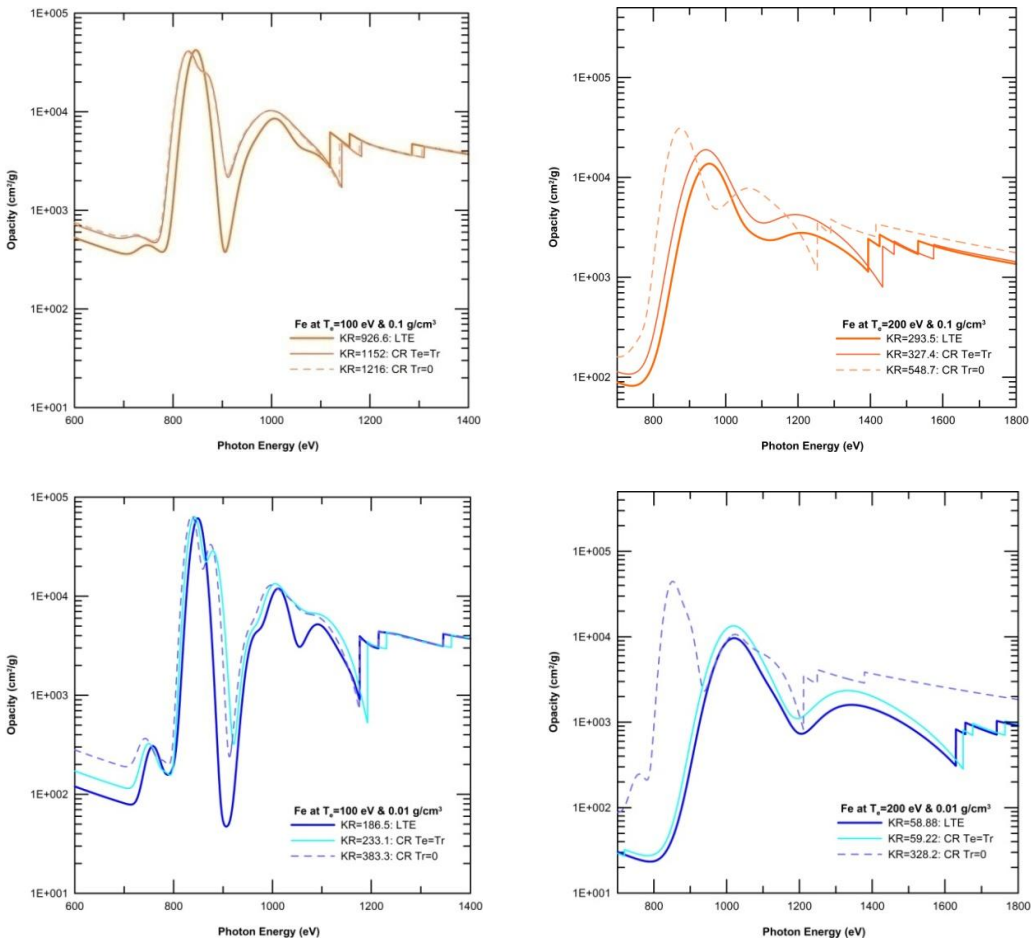

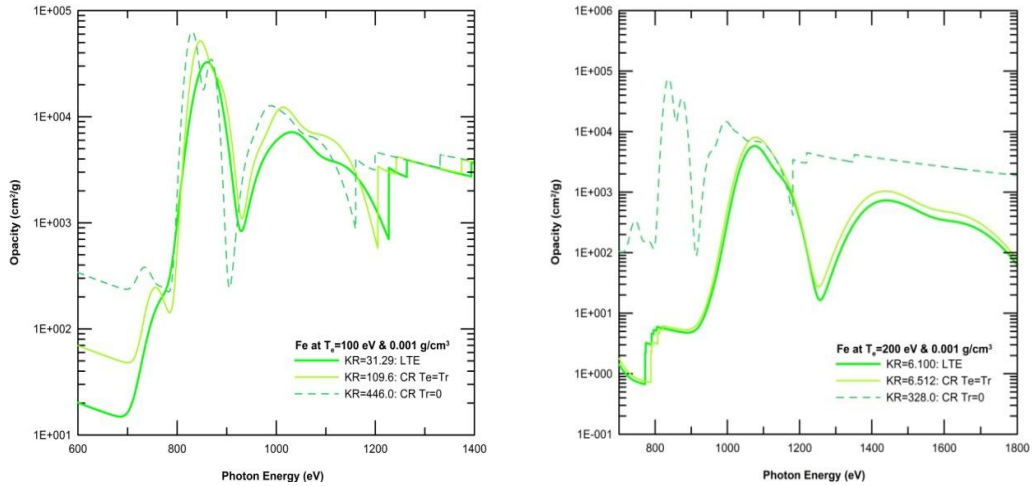

Fig. 10.c. Fe plasmas spectral opacity at electronic temperature 100/200 eV with ATMED LTE and density (a) ρ = 0.1 (—), (b) 0.01 (—), (c) 0.001 g/cm^3 (—), and also with ATMED CR for UTA formalism with radiation temperature T_R=T_e (thinner lines), T_R= 0 eV (dashed lines)

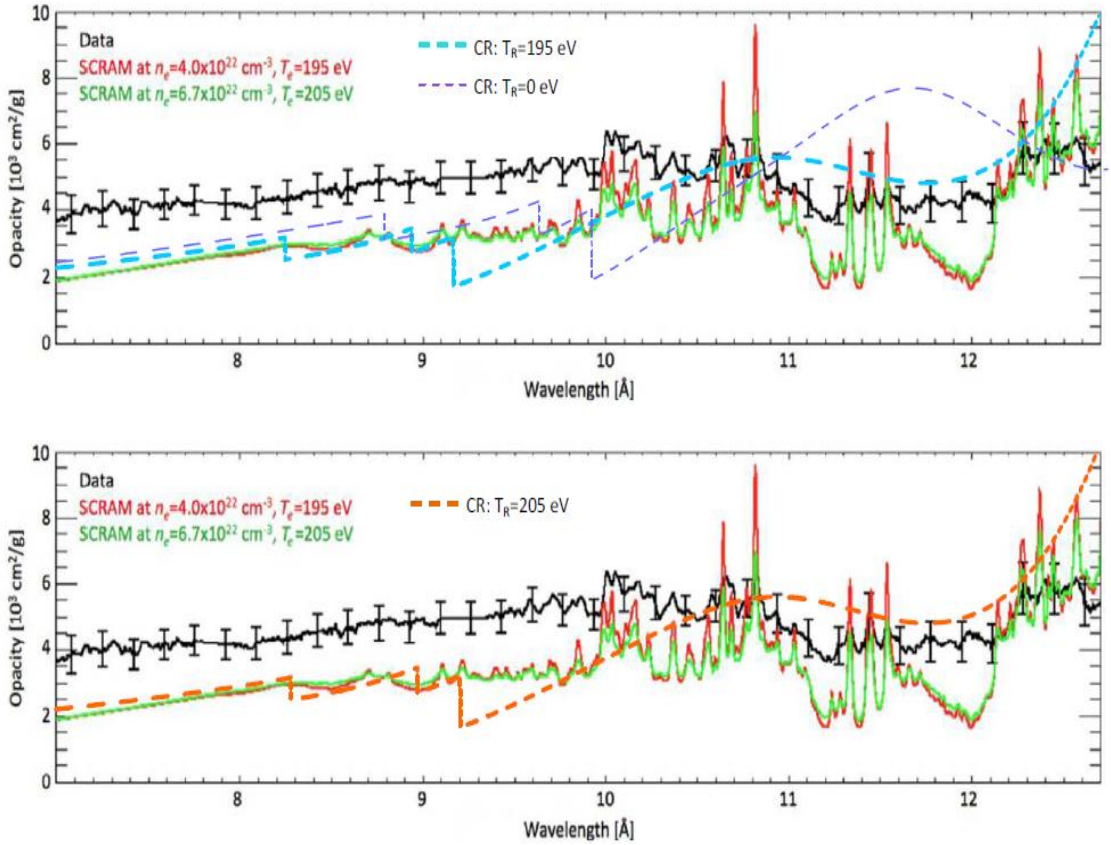

Fig. 11.a. Experimentally measured (Data) resolved opacity of Fe plasmas at electronic temperatures T_e = 195, 205 eV and density N_e = 4.0x10^{22}, 6.7x10^{22} cm^{-3} respectively with code SCRAM [34] and ATMED CR UTA, T_e = 195 (—,—) or 205 (—) eV, radiation temperature T_R

In Fig. 12 there are displayed frequency resolved opacities (cm^2/g) of iron plasma for conditions of stellar envelopes. The opacity profile of ATMED CR with $T_e=T_R$ (—) is superimposed over spectra of Ref. [35], or profiles with $T_e=T_R$ (—) or $T_R=0$ eV (—) for visualizing non-LTE effects are superimposed over spectra of Ref. [38]. The codes STA and ATMED CR, show UTA spectral structures more simple and shifted in energy with respect to the detailed codes HULLAC, LEDCOP, OPAS, SCO-RCG due to the more simplified degree of description of atomic structure and the great quantity of separated lines in the spectrum. ATMED has spectral characteristics which are an average of the profiles of different codes with variations up to 50% in the intensity of some transitions.

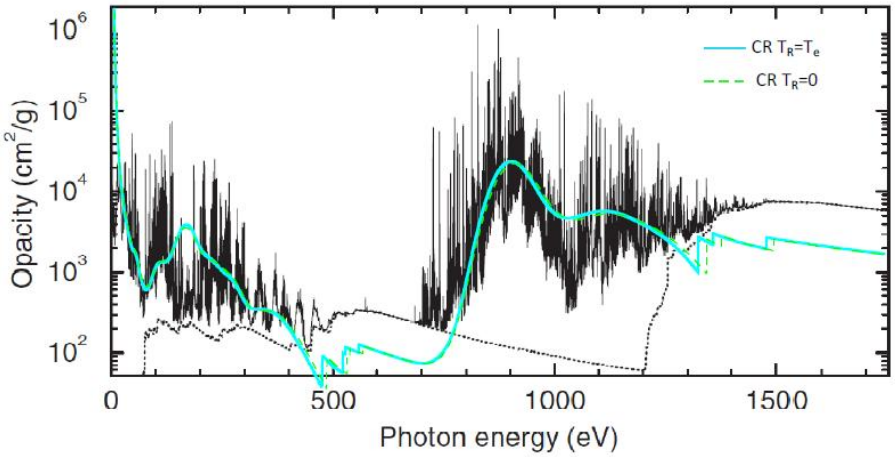

Fig. 11.b. Spectrally resolved opacity of iron plasma at electronic temperature T_e = 156 eV and electronic density $N_e = 6.9 \times 10^{21}$ cm^{-3} of code in Reference [31] and ATMED CR considering UTA formalism and also as radiation temperature T_R = 156 (—) or T_R = 0 (—) eV

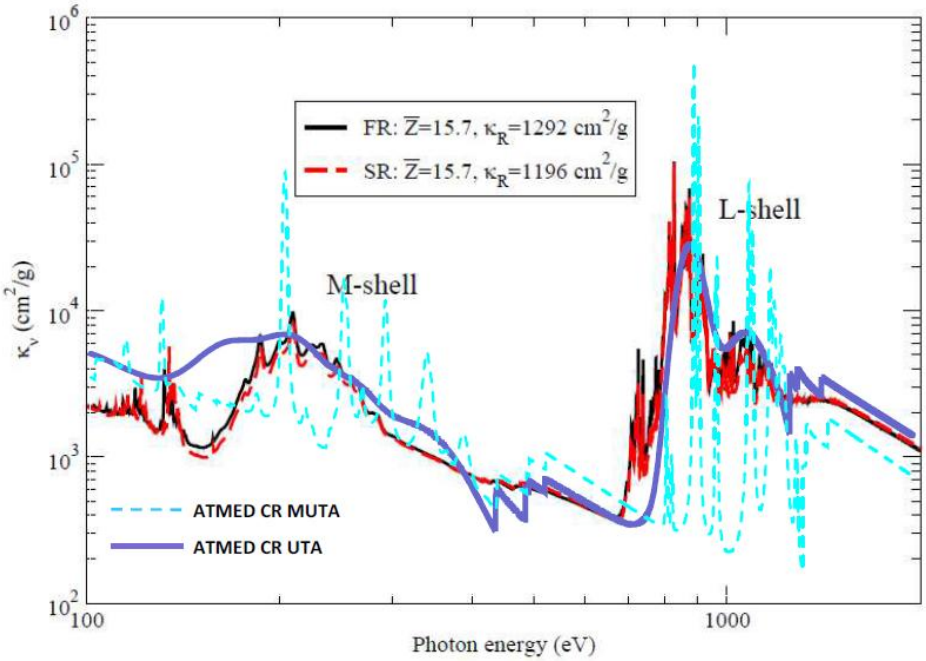

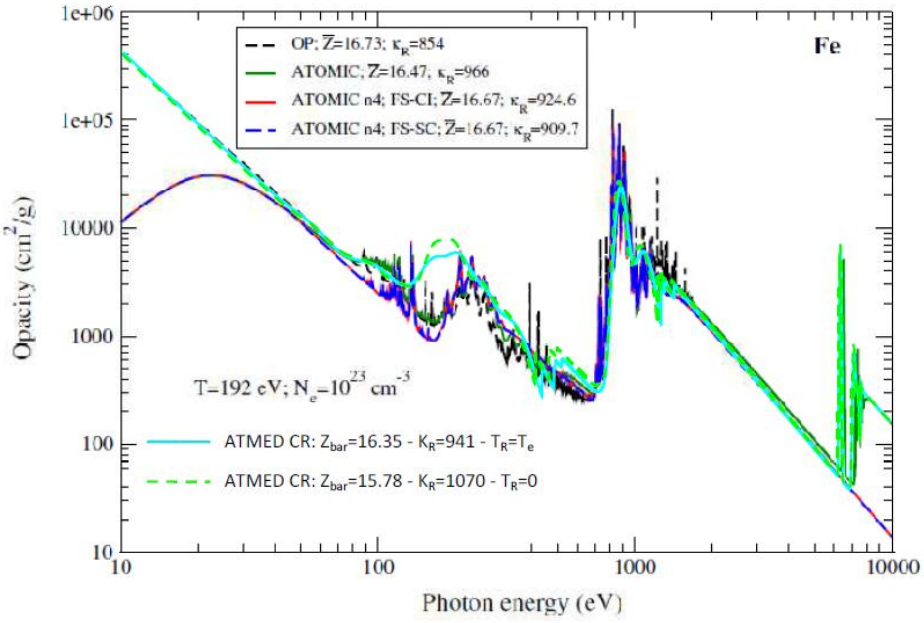

Fig. 11.c. Spectral opacity of iron plasma at electronic temperature T_e = 193/192 eV and electronic density $N_e = 10^{23}$ cm^{-3} of code ATOMIC [32,33,38] fully relativistic (FR), semi-relativistic (SR) modes and ATMED CR considering $T_e=T_R$= 193/192/0 eV. Opacity at same conditions with ATMED CR UTA (—) or MUTA (—) (above) or ATMED UTA (—) considering also T_R = 192 (—) or T_R = 0 (—) eV (below)

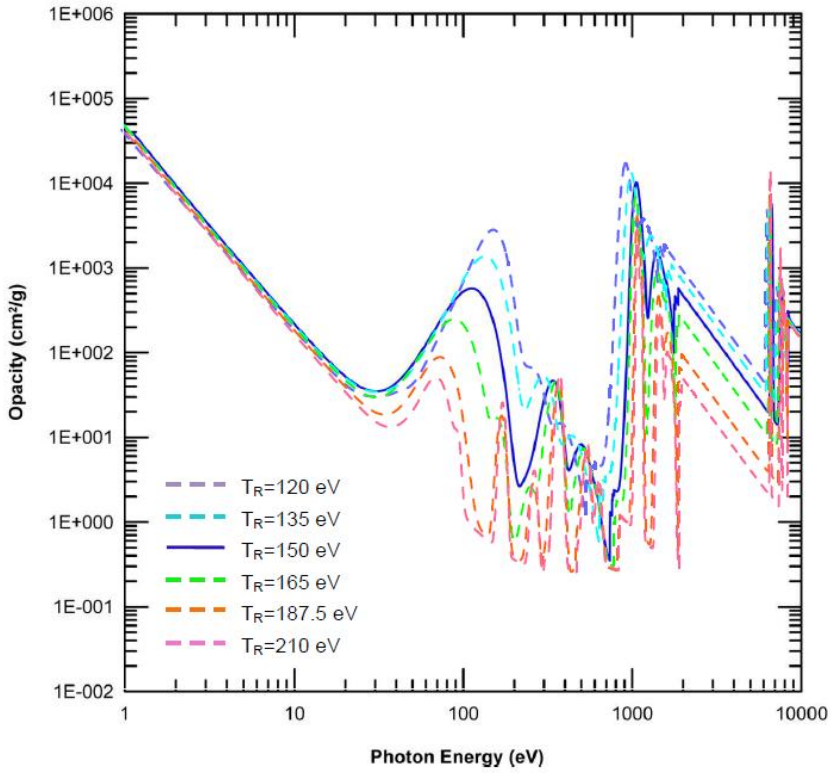

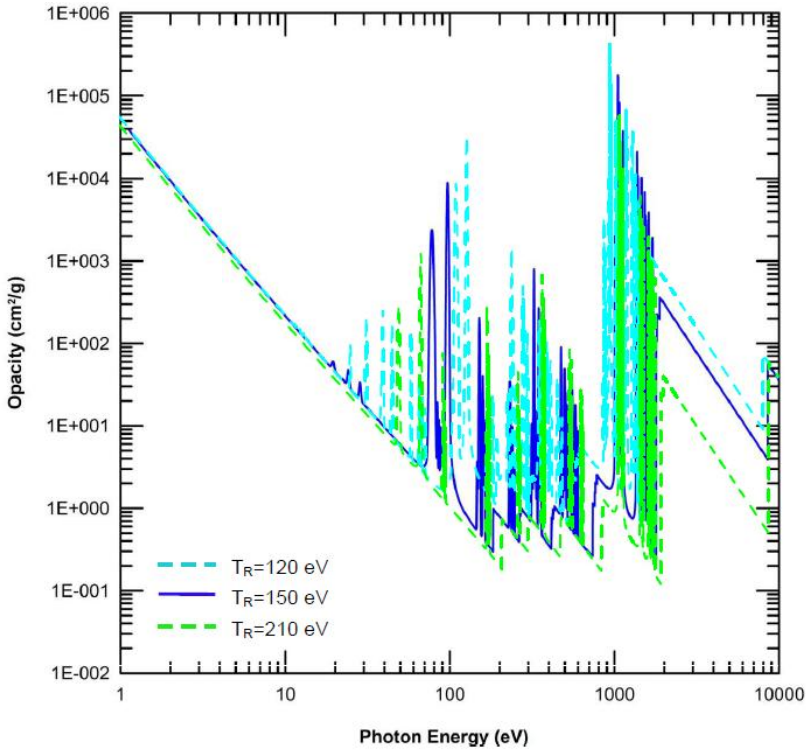

Fig. 11.d. Opacity of iron plasma at electronic temperature T_e = 150 eV, density N_e = 2E+19 cm^{-3} of ATMED UTA (above), MUTA (below)

3.2.3 Trends of Rosseland & Planck Mean Opacities

In Figs. 13-14 there are displayed graphs of trends of Rosseland and Planck mean opacities (cm^2/g) of iron plasmas, checking the high concordance of values of ATMED LTE and ATMED CR (T_e=T_R) with respect to Ref. [27], Tables 4-5. ATMED CR results for Rosseland K_R (—) and Planck K_P (—) mean opacities are similar to those of the set of codes of Ref. [27] computed with equal electronic and radiation temperatures (T_e=T_R) eV.

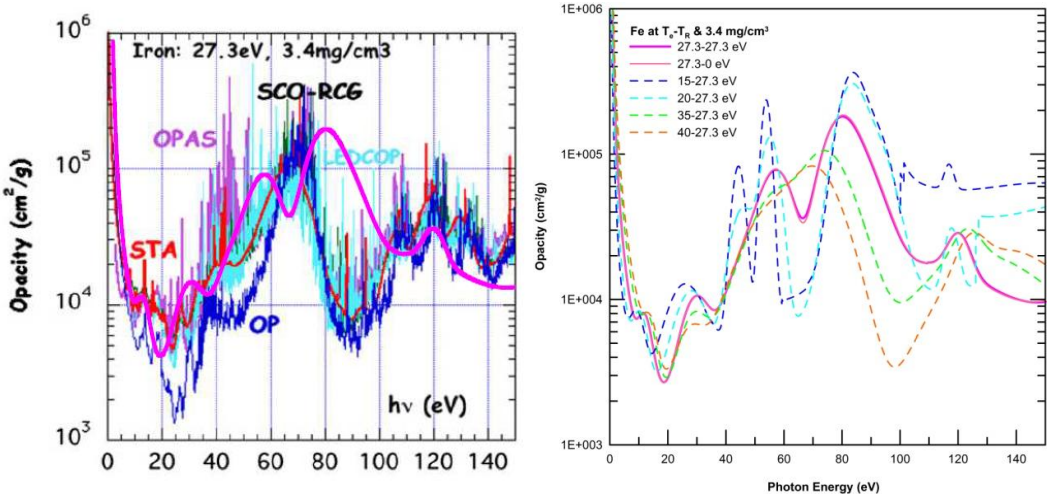

Fig. 12.a. Opacity with ATMED CR UTA (—) of iron plasmas and codes of Ref. [35], several values of T_e and matter density 3.4 mg/cm^3

Table 3.b. Rosseland mean opacity K_R (cm^2/g) and mean charge with ATMED CR at several electronic-radiation temperatures in eV.

ATMED CR UTA (T_e - T_R)	**(27.3 - 27.3)**	**(27.3 - 0)**	**(15 - 27.3)**	**(20 - 27.3)**	**(35 - 27.3)**	**(40 - 27.3)**
K_R cm^2/g	1.915E+04	1.939E+04	3.654E+04	2.699E+04	1.349E+04	9.735E+03
Mean Charge Z_{bar}	8.338317E+00	8.275221E+00	5.699154E+00	6.736098E+00	9.946713E+00	1.085547E+01

Table 4. Evolution of mean opacities with ATMED CR for comparison with codes of Fig. 13

ATMED CR: T_e = T_R = 20 eV	**5 x 10^{-6} g/cm^3**	**10^{-5} g/cm^3**	**10^{-4} g/cm^3**	**10^{-3} g/cm^3**	**10^{-2} g/cm^3**	**10^{-1} g/cm^3**
Rosseland K_R	1.661E+03	2.411E+03	8.186E+03	1.774E+04	3.477E+04	6.320E+04
Planck K_P	4.188E+04	4.436E+04	5.264E+04	6.153E+04	7.353E+04	1.015E+05
ATMED CR: T_e = 20 & T_R = 0 eV	**5 x 10^{-6} g/cm^3**	**10^{-5} g/cm^3**	**10^{-4} g/cm^3**	**10^{-3} g/cm^3**	**10^{-2} g/cm^3**	**10^{-1} g/cm^3**
Rosseland K_R	3.103E+03	3.503E+03	7.341E+03	1.777E+04	3.495E+04	6.319E+04
Planck K_P	6.910E+04	6.613E+04	5.992E+04	6.271E+04	7.374E+04	1.015E+05

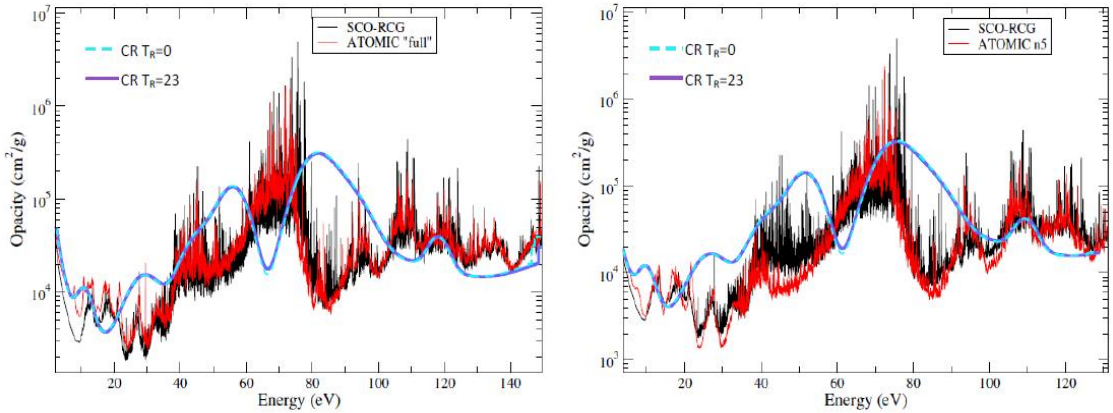

Fig. 12.b. Opacity of iron plasmas with detailed codes SCO or ATOMIC [38] and ATMED CR at electronic temperature T_e=23 eV, radiation temperature T_R and density 2 mg/cm^3, averaging with two shifted UTA structures the main groups of lines centered at around 42 or 65 eV.

The departures from LTE regime are clearly observed when computing with ATMED CR for low densities and T_R = 0 eV, K_R (—) and K_P (—) mean opacities. For the low density of ρ = 0.001 g/cm^3, ATMED CR results with T_e=T_R eV for K_R (■) and K_P (■) mean opacities are similar also to those of Ref. [27].

ATMED LTE results for K_R (■) and K_P (■) mean opacities at 10^{-4} g/cm^3 are similar to those of [27].

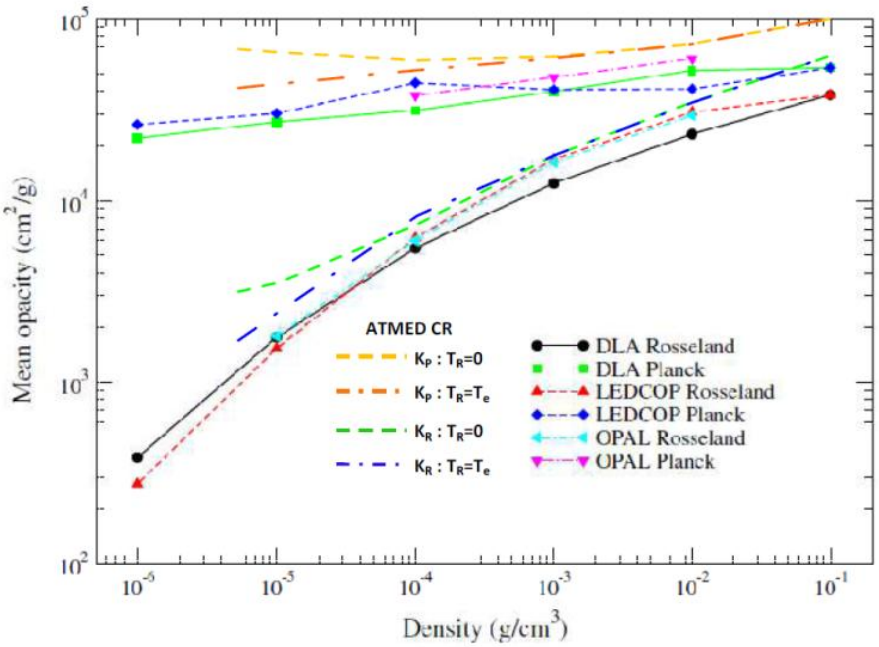

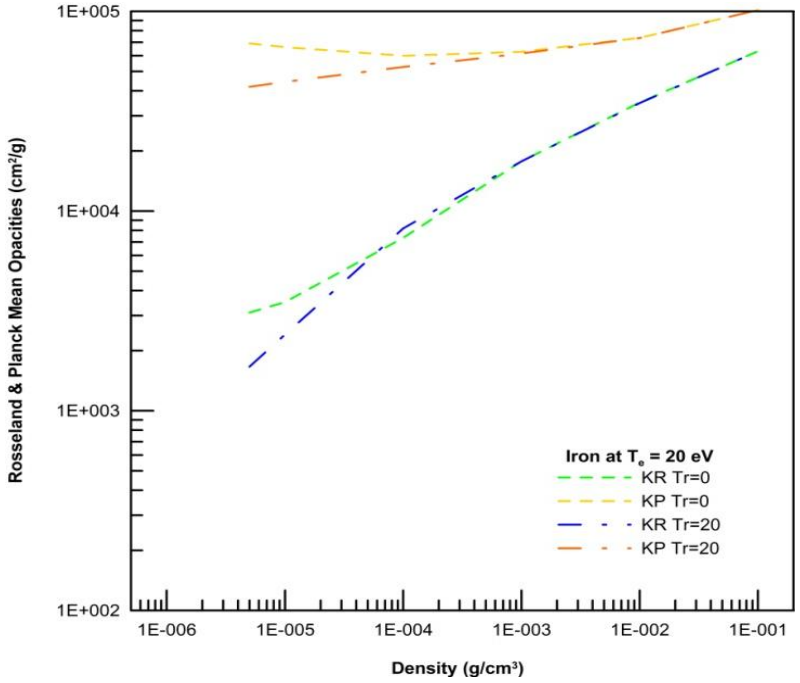

Fig. 13.a. Fe plasmas K_R and K_P mean opacities (cm^2/g) of ATMED LTE/CR and other codes of Ref. [27] at 20 eV

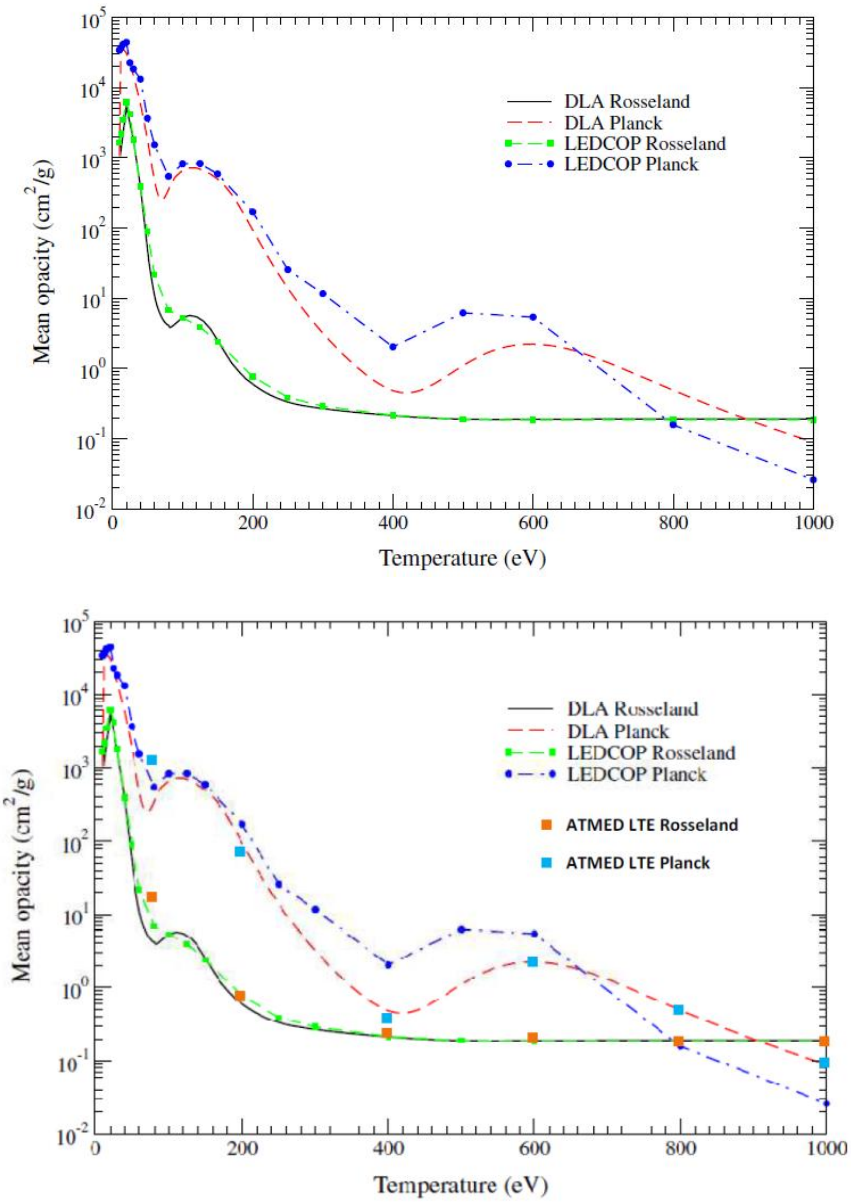

Fig. 13.b. Fe plasmas K_R and K_P mean opacities (cm^2/g) of ATMED LTE and other codes of Ref. [27] at 0.0001 g/cm^3

ATMED LTE results for K_R (■) and K_P (■) mean opacities at $10^{-2}/10^{-4}$ g/cm^3 are similar to those of Reference [27].

3.2.4 Spectrally Resolved Transmission

In Figs. 15-18 there are displayed spectra of frequency resolved transmission of iron plasmas, checking the high spectral quality of ATMED CR with respect to other atomic codes [35-38], as well as the high sensitivity to slight changes in temperatures, densities or plasma lengths.

In Fig. 17 it can be noticed also the high convergence between spectra calculated with both options for thick plasmas of ATMED CR: photon confinement probability applied to radiative rates in photoionized plasmas (T_e and $T_R \neq 0$ eV), or escape factors by bound-bound line applied to spontaneous emission without radiation field ($T_R = 0$).

Table 5.a. Evolution of mean opacities with ATMED CR UTA (T_e, T_R eV) for comparison with codes of Fig. 13

10^{-4} g/cm^3 & $T_R=T_e$	T_e = 50 eV	T_e = 80 eV	T_e = 100 eV	T_e = 200 eV	T_e = 400 eV	T_e = 600 eV	T_e = 800 eV
Rosseland K_R	2.020E+02	1.350E+01	7.714E+00	7.661E-01	2.304E-01	1.976E-01	1.942E-01
Planck K_P	2.802E+03	1.072E+03	9.078E+02	9.275E+01	4.272E-01	2.112E+00	4.967E-01
10^{-4} g/cm^3 & T_R=0	**T_e = 50 eV**	**T_e = 80 eV**	**T_e = 100 eV**	**T_e = 200 eV**	**T_e = 400 eV**	**T_e = 600 eV**	**T_e = 800 eV**
Rosseland K_R	4.025E+03	1.815E+03	1.370E+03	4.559E+02	3.702E+02	2.541E+02	1.708E+02
Planck K_P	1.117E+04	5.567E+03	4.245E+03	4.113E+03	3.263E+03	1.885E+03	1.150E+03

Table 5.b. Evolution of mean opacities with ATMED CR UTA (T_e, T_R eV) or ATMED LTE for comparison with codes of Fig. 14

10^{-2} g/cm^3 - ATMED LTE	T_e = 80 eV	T_e = 200 eV	T_e = 400 eV	T_e = 600 eV	T_e = 800 eV	T_e = 1000 eV
Rosseland K_R	5.5553E+02	5.8886E+01	2.9514E+00	6.1134E-01	3.3963E-01	2.7846E-01
Planck K_P	2.4149E+03	9.5787E+02	2.3458E+01	6.0958E+00	1.4494E+01	7.0852E+00
10^{-2} g/cm^3 CR & $T_R=T_e$	**T_e = 80 eV**	**T_e = 100 eV**	**T_e = 200 eV**	**T_e = 600 eV**	**T_e = 800 eV**	**T_e = 1000 eV**
Rosseland K_R	6.040E+02	2.520E+02	5.922E+01	6.278E-01	3.473E-01	2.821E-01
Planck K_P	2.993E+03	1.883E+03	1.390E+03	6.703E+00	1.494E+01	7.419E+00
10^{-2} g/cm^3 CR & T_R=0	**T_e = 80 eV**	**T_e = 100 eV**	**T_e = 200 eV**	**T_e = 600 eV**	**T_e = 800 eV**	**T_e = 1000 eV**
Rosseland K_R	9.940E+02	3.833E+02	3.325E+02	1.926E+02	1.416E+02	1.041E+02
Planck K_P	3.937E+03	2.253E+03	3.809E+03	1.340E+03	8.409E+02	5.275E+02
10^{-4} g/cm^3 - ATMED LTE	**T_e = 80 eV**	**T_e = 200 eV**	**T_e = 400 eV**	**T_e = 600 eV**	**T_e = 800 eV**	**T_e = 1000 eV**
Rosseland K_R	1.0695E+01	7.2892E-01	2.2502E-01	1.9563E-01	1.9379E-01	1.9356E-01
Planck K_P	1.0171E+03	6.6086E+01	3.3925E-01	2.0875E+00	4.8866E-01	8.8886E-02

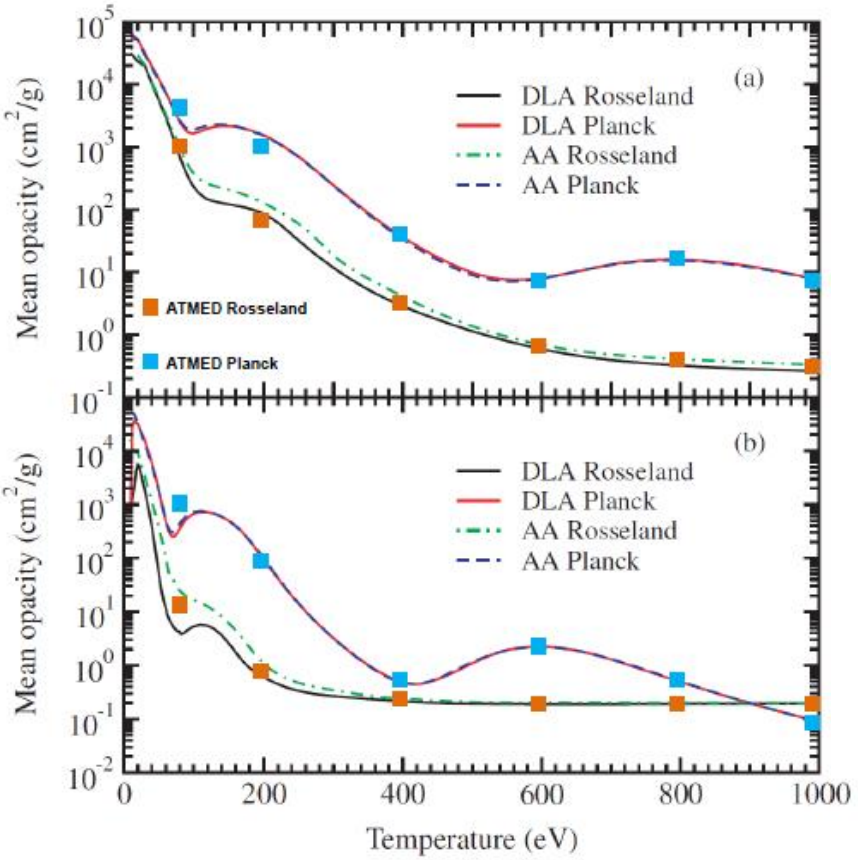

Fig. 14. Iron plasmas mean opacities with ATMED LTE, K_R (■) and K_P (■) cm²/g and code DLA of Ref. [27]: (a) 0.01, (b) 0.0001 g/cm³.

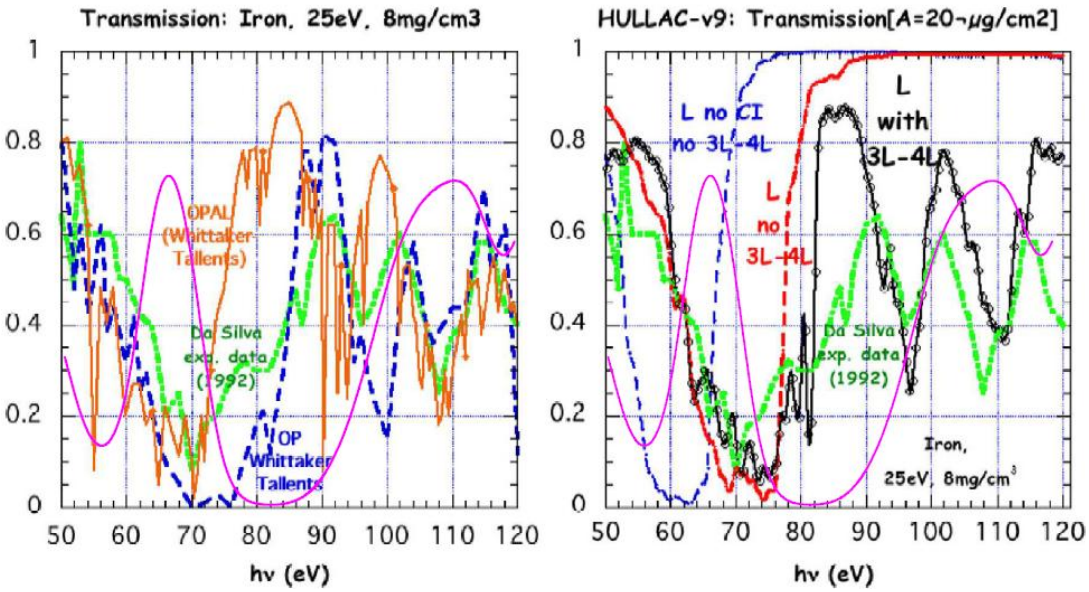

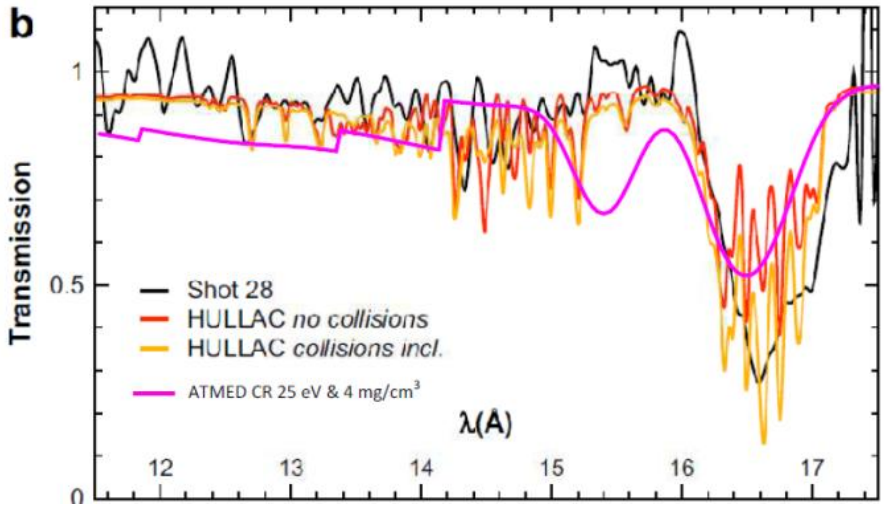

Fig. 15. Fe experimental transmission (Da Silva 1992) compared to OPAL, OP [35] and ATMED CR (—) at 8 mg/cm^3, 25 eV, D=2.5E-3 cm, 20 μg/cm^2 averaging with a slightly shifted UTA structure the main group of lines centered at around 70, 96 or 108 eV (above). Fe experimental transmission (shot 28) compared to HULLAC [36] and ATMED CR (—) at 4 mg/cm^3, 25 eV, D=5E-3 cm, 20 μg/cm^2 (below)

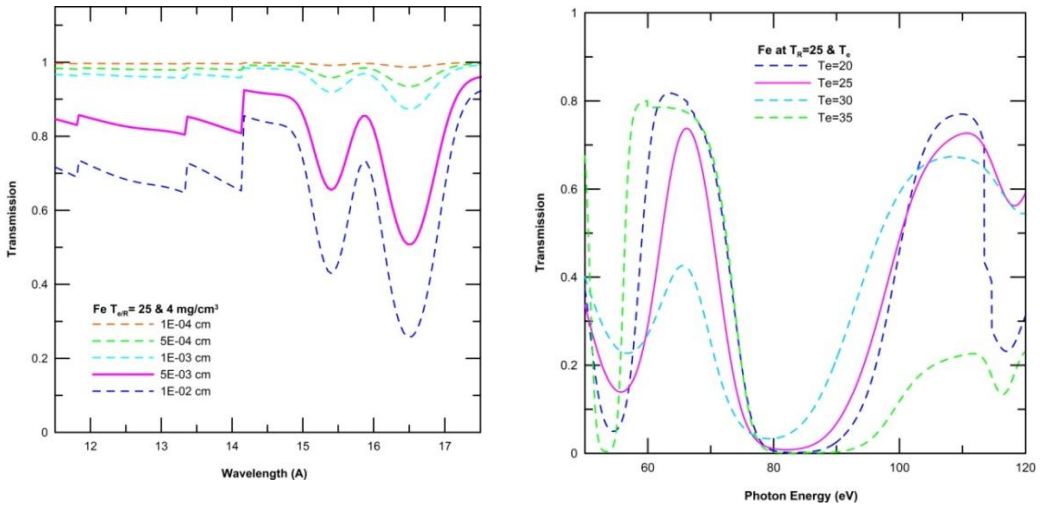

Fig. 16. Fe transmission with ATMED CR at T_R = 25 eV, 20 μg/cm^2: 4 mg/cm^3 and other lengths (left) or 8 mg/cm^3 and other T_e (right)

3.2.5 Radiative properties of mixtures with iron

In Figs. 19-20 there are displayed spectra of frequency resolved transmission and opacity (cm^2/g) of iron plasmas inside mixtures, checking the high spectral quality of ATMED CR with respect to other atomic codes [39,40], as well as the high sensitivity to slight changes in temperatures, densities or number of components.

The transmission of mixture Fe+Mg computed with ATMED CR as in Fig. 19 shows clearly two UTA shifted structures, one for lines Heα, Lyα and the other for lines Lyα, Heβ.

In Figs. 20-21 there can be observed the departures from LTE in solar plasma computing with ATMED LTE (—) or ATMED CR considering 10 components (—), or 18 (—) as in Table 6. The mixture of 10 elements has 92.0823% of hydrogen, and the other first nine components

with the same percentages. In the boundary of convection-radiation zone at mixture conditions $T_e=T_R=193$ eV and $N_e=$ 1E+23 cm^{-3}, low Z elements are in frontier regions of regimes NLTE-LTE and intermediate-high Z elements as iron are practically in LTE regime.

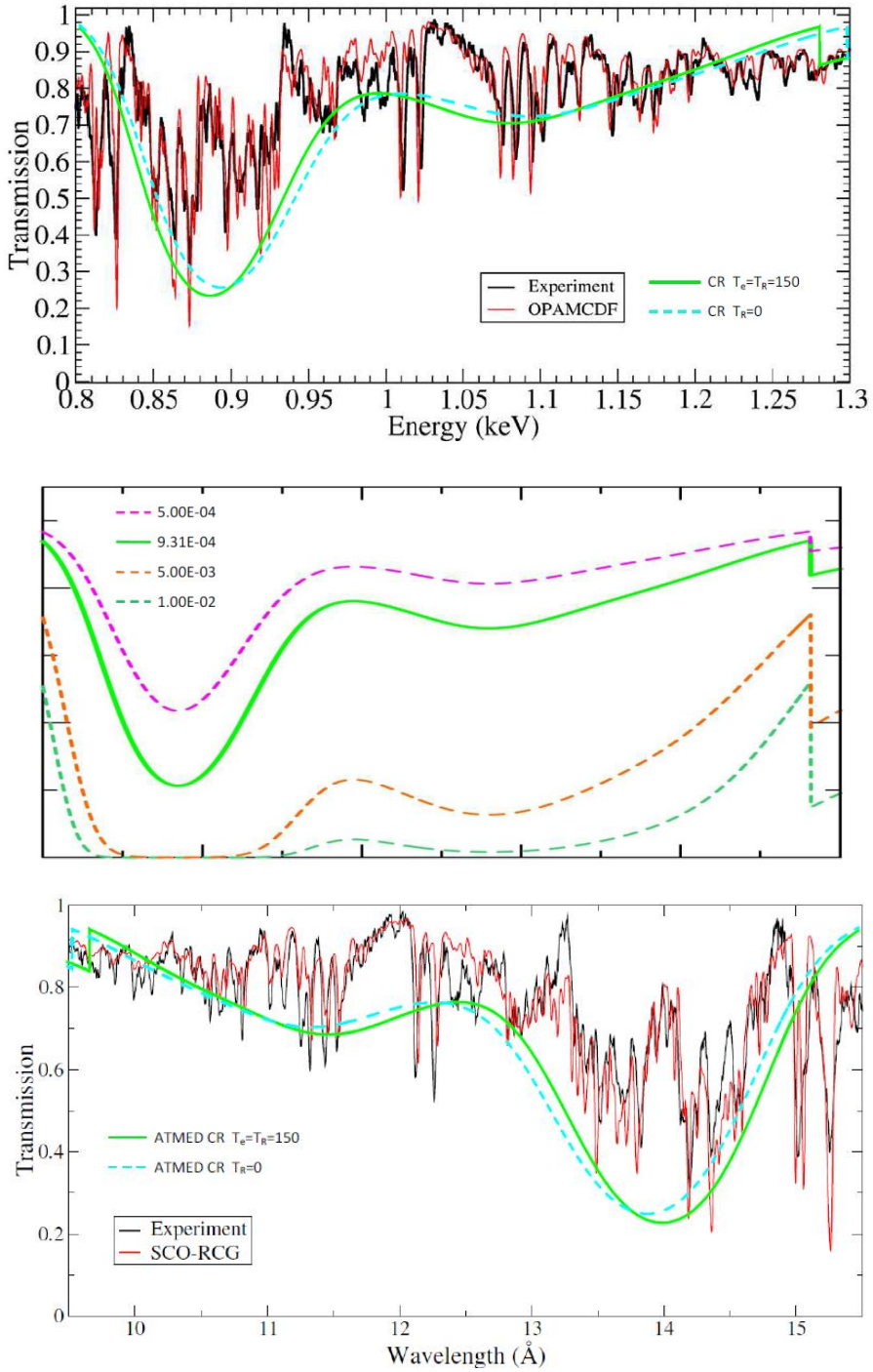

Fig. 17. Fe experimental transmission compared to codes OPAMCDF, SCO-RCG [37,38] and ATMED CR at 0.058 g/cm^3, 150 eV, 54 µg/cm^2, corresponding to plasma length of 9.31E-04 cm. Intermediate figure with same scale and plasma lengths in range 5E-04÷1E-02 cm

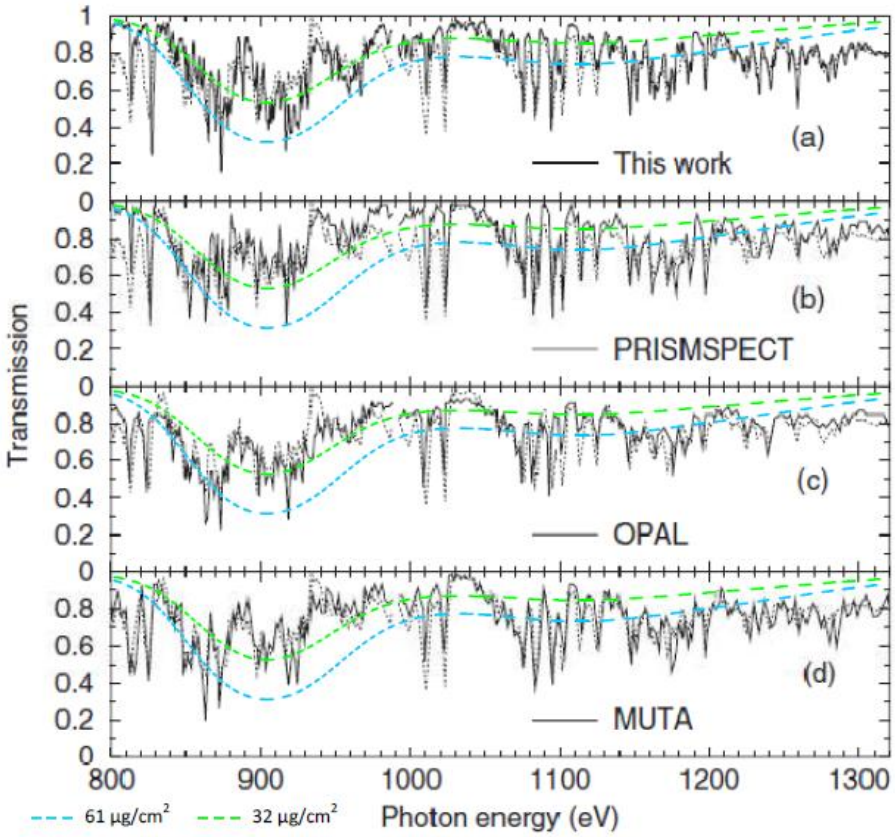

Fig. 18.a. Spectrally resolved transmissions of iron plasma at electronic temperature $T_e = T_R$ = 156 eV and density $N_e = 6.9 \times 10^{21}$ cm^{-3} of codes OPAL, PRISMSPECT in Reference [31] and ATMED CR considering UTA formalism and also as areal density 61 (—) or 32 (—) µg/cm^2

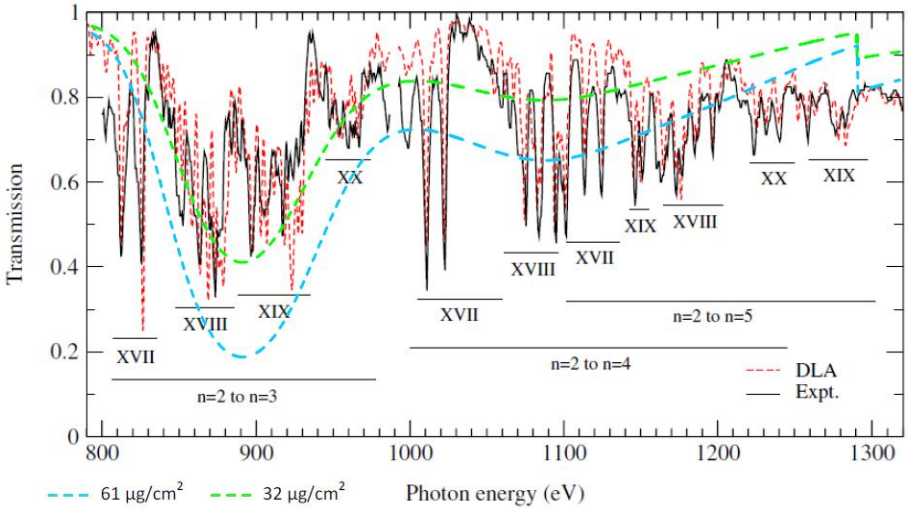

Fig. 18.b. Spectral experimental transmission of iron plasma at electronic temperature $T_e = T_R$ = 150 eV and density $N_e = 8.5 \times 10^{21}$ cm^{-3} compared to DLA code in Reference [27] and ATMED CR considering UTA formalism and also as areal density 61 (—) or 32 (—) µg/cm^2

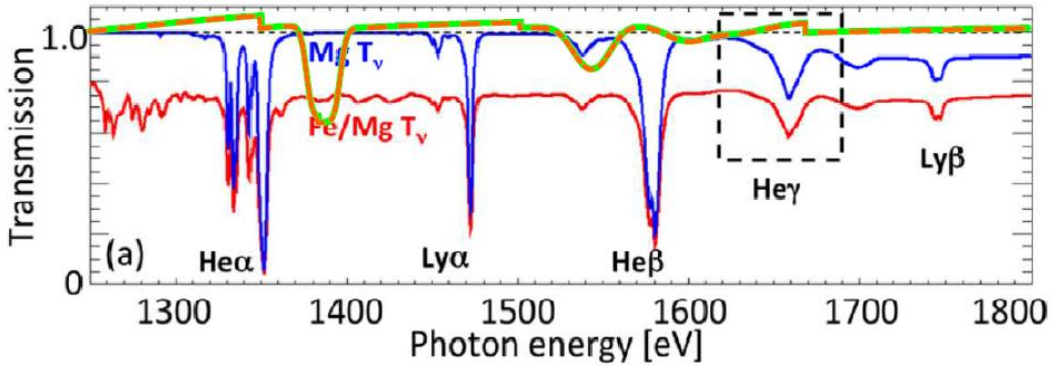

Fig. 19. Mixture FeMg transmission computed with RADIATOR + GALM [39] and compared to the calculated of ATMED CR at electronic density N_e = 8.0 x 10^{21} cm^{-3}, T_e = 165 eV and as radiation temperature T_R = 165 eV (—) or T_R = 0 eV (—) with areal density 7.4E+17 ion/cm^2

Table 6. Solar plasma considering a mixture of 18 components and their volume percentage %

Element	%H	%He	%O	%Fe	%Mg	%N
Percentage (%)	92.0808	7.8	0.061	0.0037	0.0024	0.0084
Element	%Si	%S	%C	%Ne	%Na	%Al
Percentage (%)	0.0031	0.0015	0.03	0.0076	1.875E-4	1.875E-4
Element	%P	%Cl	%Ti	%Cr	%Mn	%Ni
Percentage (%)	1.875E-4	1.875E-4	1.875E-4	1.875E-4	1.875E-4	1.875E-4

The non-LTE effects are accounted for with the collisional radiative balance rising fundamentally the hydrogen opacity slope with respect to compute in LTE regime or with Saha equations, increasing the Rosseland mean opacities also of other light elements and lowering the total mean charge [40,41].

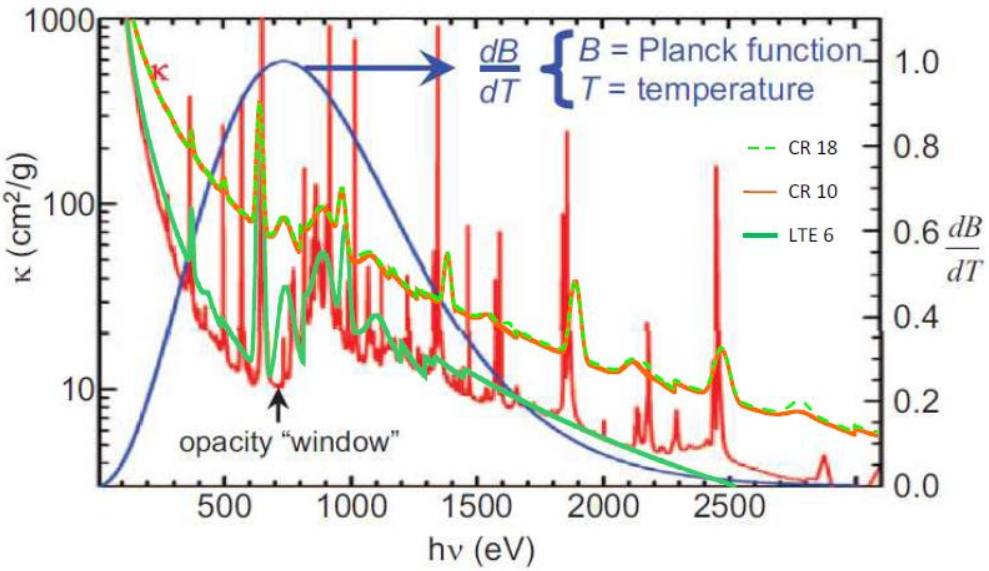

Fig. 20. Mixture of solar plasma with Fe computed with ATMED LTE and 6 components (—), ATMED CR with 10 (—) or 18 (—) components with composition of Ref. [41] or with code (—) of Ref. [40] at N_e = 1.0 x 10^{23} cm^{-3}, T_e = 193 eV (convection boundary region)

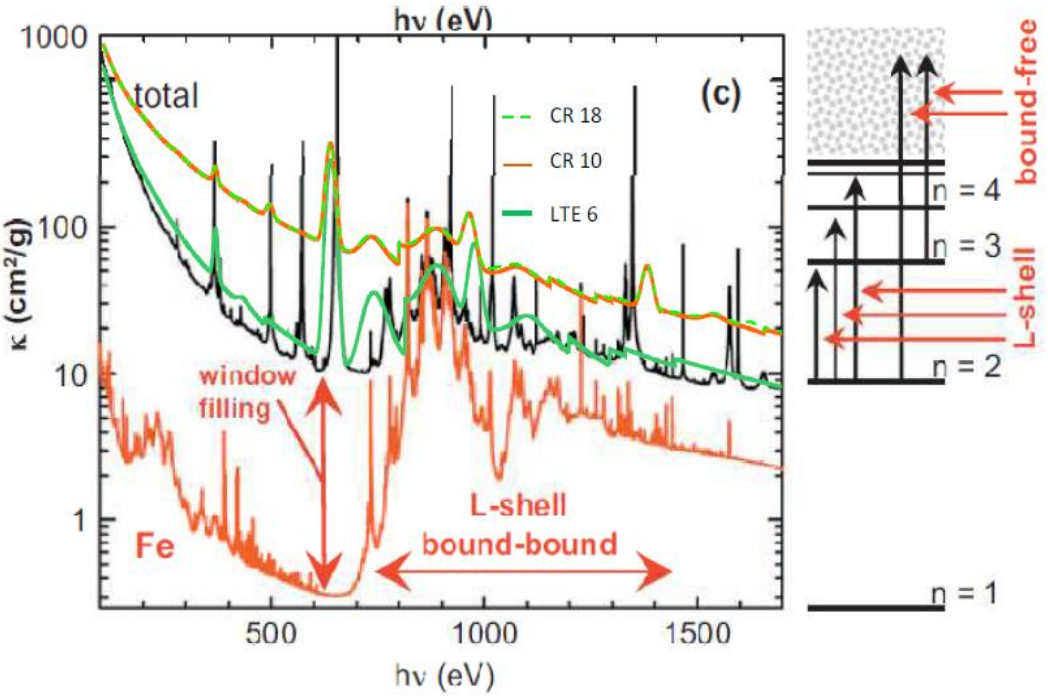

Fig. 21. Mixture of solar plasma with Fe computed with ATMED LTE and 6 components (—), ATMED CR with 10 (—) or 18 (—) components with composition of Ref. [41] or with code (—) of Ref. [40] at N_e = 1.0 x 10^{23} cm^{-3}, T_e = 193 eV (convection boundary region)

4. SUMMARY AND CONCLUSIONS

In this paper, there are modeled with ATMED CR iron steady state plasmas for wide thermodynamic ranges, proposed in theoretical calculations or real experiments in high energy density facilities. The results for plasma properties can be considered as very optimal and accurate, according to the electronic and radiation temperatures – density points of conditions provided in bibliographic data. The iterative loops implemented inside the stationary module of ATMED CR without matricial resolution following A.F. Nikiforov et al. [14], are very rapid and useful for calculating statistical averaged plasma properties, avoiding some of the typical difficulties encountered when interpreting the simulation of plasmas created in laboratories or in computational experiments as for example, intensive calculations with enormous matrices of detailed collisional radiative codes. This article has displayed also the fundamental chronology of average atom models evolution as a consequence of the gradual quantization of matter atomic structure through decades.

The present work contains a representative sample of steady state iron plasmas, highlighting the huge computation capability extension up to millions of plasmas with the implementation of a collisional radiative balance in the relativistic average atom model ATMED [4-7]. The departures from LTE regime are clearly observed when plasma properties are computed with module ATMED CR (T_R = 0 eV or $T_R \neq T_e$ eV) in respect of calculating with ATMED CR ($T_e = T_R$). The non-LTE effects for all cases are more significant with decreasing densities and increasing temperatures depending on the atomic number of the element, intrinsic characteristic behavior of plasma conditions which in turn is also very well reproduced by ATMED CR code. Inside the thesis book [2,42] more data of iron plasmas can be found illustrating the extension of computation capability with cases also contained inside other References [10,17,30,43]. There is a good agreement of atomic and radiative properties with respect to very recent experimental measurements of laboratories simulated by other codes [44] and to the last theoretical developments in quantum mechanics of statistical methods and state of the art models,

confirming tested high robustness and reliability of ATMED model software.

ACKNOWLEDGEMENTS

This work has been partially supported by a Research Project of the Spanish Ministry of Science and Innovation (ENE2009-11208), by a Research Project of the "Agencia Canaria de Investigación, Innovación y Sociedad de la Información" of the regional government of the Canary Islands. (SOLSUBC2008000057) and also by the "Keep-in Touch" project of the European Union. The authors thankfully acknowledge the computer resources from Atlante, technical expertise and assistance provided by the Spanish SupercomputingNetwork (RES) and Instituto Tecnológico de Canarias Gobierno de Canarias.

COMPETING INTERESTS

Author has declared that no competing interests exist.

REFERENCES

1. Benita AJ, Mínguez E, Mendoza MA, Rubiano JG, Gil JM, Rodríguez R, Martel P. Collisional radiative average atom code based on a relativistic screened hydrogenic model. High Energy Density Physics. 2015;14:18-29.
2. Benita AJ. Collisional radiative average atom code with relativistic atomic model. Theoretical physics. LAP Lambert Academic Publishing; 2017.
   ISBN: 978-620-2-01943-9
3. A.J. Benita. Fast calculation of plasmas properties with ATMED LTE. Project of Nuclear Science and Technology Master at UPM; 2012.
4. Mendoza MA, Rubiano JG, Gil JM, Rodriguez R, Florido R, Benita AJ, Martel P, Minguez E. Fast computation of radiative properties and EOS of warm dense matter using the ATMED code. Eight International Conference on Inertial Fusion Sciences and Applications (IFSA 2013). Nara, Japan; 2013.
5. Mendoza MA, Rubiano JG, Gil JM, Rodriguez R, Florido R, Espinosa G, Martel P, Minguez E. Calculation of radiative opacity of plasma mixtures using a relativistic screened hydrogenic model. Journal of Quantitative Spectroscopy & Radiative Transfer. 2014;140:81–98.
6. Mendoza MA, Rubiano JG, Gil JM, Rodriguez R, Florido R, Martel P, Minguez E. A new set of relativistic screening constants for the screened hydrogenic model. HEDP. 2011;7:169–179.
7. Ruano FH, Rubiano JG, Mendoza MA, Gil JM, Rodriguez R, Florido R, Martel P, Minguez E. Relativistic screened hydrogenic radial integrals. Journal of Quantitative Spectroscopy & Radiative Transfer. 2012;117:123-132.
8. Lokke WA, Grasberger WH. XSNQ-U A Non-LTE emission and absorption coefficient subroutine. Prepared for U.S. Energy Research & Development Administration under contract No. W-7405-Eng-48, UCRL-52276; 1977.
9. Joseph Abdallah, et al. The reduced detailed configuration accounting (RDCA) model for NLTE plasma calculations. High Energy Density Physics. 2008;4:124–130.
10. Faussurier G, Blancard C, Kato T, More RM. Prigogine theorem of minimum entropy production applied to the average atom model. High Energy Density Physics. 2009;5:283–293.
11. Faussurier G, et al. Nonlocal thermo-dynamic equilibrium self-consistent average-atom model for plasma physics. Physical Review E. 2001;63:026401.
12. Balazs F. Rozsnyai. Collisional radiative average atom model for hot plasmas. Physical Review E. 1996;55.
13. Balazs F. Rozsnyai. Hot plasma opacities in the presence or absence of local thermodynamic equilibrium. High Energy Density Physics. 2010;6:345–355.
14. Nikiforov AF, Novikov VG, Uvarov VB. Quantum-statistical models of hot dense matter. Methods for Computation Opacity and Equation of State. Birkhäuser Verlag; 2005.
15. Benita AJ. Calculation of temporal plasmas of XFEL experiments with a relativistic collisional radiative average atom code. Physical Science International Journal; 2018.
    DOI: 10.9734/PSIJ/2018/40246
16. Robin Piron. Atome moyen variationnel dans les plasmas quantiques. Physics. Commissariat A l'Energie Atomique. HAL; 2009.
    Id: <tel-00446558>

17. The 9th NLTE Code Comparison Workshop. Paris, France; 2015.
Available:http://nlte.nist.gov/NLTE9/
18. Piron R, et al. Review of the 9th NLTE code comparison workshop. High Energy Density Physics. 2017;23:38–47.
19. Aguiar JC, Di Rocco HO. The combined use of screening and quantum defect parameters in the study of ionized atoms. High Energy Density Physics. 2015;14:13–17.
20. Liberman DA. INFERNO: A better model of atoms in dense plasmas. J. Quant. Spectrosc. Radiat. Transf. 1982;27(3):335.
21. Crowley BJB, Harris JWO. Modeling of plasmas in an average-atom local density approximation: The CASSANDRA code. J. Quant. Spectrosc. Radiat. Transf. 2001;71: 257.
22. Pattison LK, et al. The calculation of free electron density in CASSANDRA. High Energy Density Physics. 2010;6:66–69.
23. Stern PA, Hansen SB, Wilson BG, Isaacs WA. Equation of state, occupation probabilities and conductivities in the average atom PURGATORIO code. High Energy Density Physics. 2007;3:278.
24. Sherrill ME, et al. NLTE Opacities of Mid- and High-Z Cocktails, LANL. American Institute of Physics; 2009.
25. Gil JM, et al. Analysis of the influence of the plasma thermodynamic regime in the spectrally resolved and mean radiative opacity calculations of carbon plasmas in a wide range of density and temperature. Journal of Quantitative Spectroscopy & Radiative Transfer. 2013;114:136–150.
26. Rodriguez R, et al. Determination of the average ionization and thermodynamic regimes of xenon plasmas with an application to the characterization of blast waves launched in xenon clusters. High Energy Density Physics. 2011;7:71–76.
27. Fengtao Jin, et al. Radiative opacity of iron studied using a detailed level accounting model. The Astrophysical Journal. 2009; 693:597–609.
28. Kouser R, et al. Quantum statistical model for hot dense matter. Conference Paper; 2015.
29. Kouser R, et al. Radiative properties of matter based on quantum statistical method. Chin. Phys. B. 2017;26(7):075-201.
30. Abdallah J, et al. The reduced detailed configuration accounting (RDCA) model for NLTE plasma spectral calculations. High Energy Density Physics. 2009;5:204–207.
31. Gao Cheng, Zeng Jiaolong. Spectrally resolved and Rosseland and Planck mean opacities of iron plasmas at temperatures above 100 eV: A systematic study. Physical Review; 2008.
32. Fontes CJ, et al. Relativistic opacities for astrophysical applications. High Energy Density Physics. 2015;16:53–59.
33. Colgan J, et al. Light element opacities from ATOMIC. High Energy Density Physics. 2013;9:369–374.
34. Nagayama T, et al. Model uncertainties of local-thermodynamic-equilibrium K-shell spectroscopy. High Energy Density Physics. 2016;20:17–22.
35. Turck-Chièze S, et al. Radiative properties of stellar envelopes: Comparison of asteroseismic results to opacity calculations and measurements for iron and nickel. High Energy Density Physics. 2013; 9:473–479.
36. Loisel G, et al. Absorption spectroscopy of mid and neighboring Z plasmas: Iron, nickel, copper and germanium. High Energy Density Physics. 2009;5:173–181.
37. Comet M, et al. A project based on multi-configuration Dirac Fock calculations for plasma spectroscopy. High Energy Density Physics. 2017;24:1–8.
38. Pain JC, et al. Detailed opacity calculations for astrophysical applications. Atoms. 2017;5:22.
DOI: 10.3390/ atoms5020022
39. Nagayama T, et al. Control and diagnosis of temperature, density and uniformity in x-ray heated iron/magnesium samples for opacity measurements. Physics of Plasmas. 2014;21:056-502.
40. Bailey JE, Rochau GA, Mancini RC, Iglesias CA, Mac Farlane JJ, Golovkin IE, Blancard C, Cosse Ph, Faussurier G. Experimental investigation of opacity models for stellar interior, inertial fusion and high energy density plasmas. Physics of Plasmas; 2009.
41. Benita AJ. Calculation of opacities for astrophysical plasmas with a relativistic collisional radiative average atom code. Elsevier; 2018.
42. Benita AJ. Book Summary; 2017.

ISBN: 978-620-2-01943-9

Available:https://www.researchgate.net/profile/Aj_Benita

43. Franklin JD, Serduke, et al. WorkOp-IV summary: Lessons from iron opacities. Journal of Quantitative Spectroscopy & Radiative Transfer; 2000.

44. Pain JC, Gilleron F. SCO-RCG collisional radiative code. High Energy Density Physics. 2015;15:30.

© 2018 Benita; This is an Open Access article distributed under the terms of the Creative Commons Attribution License (http://creativecommons.org/licenses/by/4.0), which permits unrestricted use, distribution, and reproduction in any medium, provided the original work is properly cited.

Peer-review history:
The peer review history for this paper can be accessed here:
http://www.sciencedomain.org/review-history/24863